Volcanic imprints in last-millennium land summer temperatures in the circum-North Atlantic area

Feng Wang[a,b], Dominique Arseneault[c,d], Étienne Boucher[b,d,e], Fabio Gennaretti[f], Francois Lapointe[g], Shulong Yu[h], Pierre Francus[a,b]

[a] *Centre Eau Terre Environnement, Institut National de la Recherche Scientifique, Québec, G1K 9A9, Canada*

[b] *GEOTOP Research Centre in the Dynamics of the Earth System, Montréal, QC H2X 3Y7, Canada*

[c] *Département de Biologie, Chimie et Géographie, Centre d'Études de la Forêt, Université du Québec à Rimouski; Rimouski, G5L 3A1, Canada*

[d] *Centre d'Études Nordiques, Université Laval, Québec, G1V 0A6, Canada*

[e] *Département de Géographie, Université du Québec à Montréal, Montréal, H2X 3R9, Canada*

[f] *Groupe de Recherche en Écologie de la MRC-Abitibi, Institut de Recherche sur les Forêts, Université du Québec en Abitibi-Témiscamingue, Amos, J9T 2L8, Canada*

[g] *Department of Geosciences, Climate System Research Center, University of Massachusetts Amherst, Amherst, Massachusetts*

[h] *Key Laboratory of Tree-ring Ecology of Uigur Autonomous Region, Key Laboratory of Tree-ring Physical and Chemical Research, Institute of Desert Meteorology, China Meteorological Administration, Urumqi, 830002, China*

Corresponding author: Feng Wang, feng.wang@inrs.ca

Early Online Release: This preliminary version has been accepted for publication in *Journal of Climate*, may be fully cited, and has been assigned DOI 10.1175/JCLI-D-23-0107.1. The final typeset copyedited article will replace the EOR at the above DOI when it is published.

ABSTRACT

Summer cooling is one of the most direct consequences of explosive volcanic eruptions that can affect ecosystems and human societies. Recent studies revealed a multi-year cooling impact on hemispheric and global summer temperatures after tropical eruptions, yet, the volcanic responses appear to vary on regional scales. Here, we revisit volcano-induced summer cooling in Eastern Canada, Northern and Central Europe by applying superposed epoch analysis on CMIP6-PMIP4 simulations and millennial temperature reconstructions based on tree-ring density. We then examine potential causes modulating region-specific volcanic impact. While confirming that, on average, tropical eruptions over the last millennium have induced a longer cooling (> 4 years) than eruptions from extratropical Northern Hemisphere in all three North Atlantic regions, we show that the peak magnitude of cooling is stronger in Eastern Canada. We also find that the detected volcanic temperature anomalies can be strongly affected by the selection and number of volcanic events and non-volcanic signals embedded in the climate time series. This study highlights the risks of using highly noisy proxy records to investigate volcanic impacts, especially in regions with strong unforced climate variability. The CMIP6-PMIP4 simulations generally agree with the three reconstructions on the average response to tropical eruptions, but their performance is poorer regarding the production of significant cooling after extratropical eruptions. Our results further suggest that the particular sensitivity to tropical eruptions in Eastern Canada is likely related to increased sea ice surrounding Quebec-Labrador associated with the positive Arctic Oscillation and North Atlantic Oscillation formed during the first post-eruption winter.

1. Introduction

Explosive volcanic eruptions are a dominant driver of the Earth's climate variability by injecting sulfur dioxide into the stratosphere, which enhances the amount of stratospheric aerosol, thus scattering incoming solar radiation and cooling surface summer temperatures (Robock 2000; Sigl et al. 2015; Gautier et al. 2019; Huhtamaa et al. 2022; Marshall et al. 2022). Significant temperature decreases caused by large eruptions can lead to tremendous environmental and socioeconomic effects (Büntgen et al. 2016; Toohey et al. 2016; Guillet et al. 2017, 2020; McConnell et al. 2020). For example, the 1815 Tambora eruption from Indonesia resulted in "the year without a summer" in Europe and northeastern North America, with snowfalls observed in June of 1816 CE in Albany and Quebec City (Oppenheimer 2003). The unusually cold conditions

Accepted for publication in *Journal of Climate*. DOI 10.1175/JCLI-D-23-0107.1.

further led to severe food and health crisis for years in North Atlantic regions (Harington 1992; Oppenheimer 2003) as well as in Eastern Asia (Gao et al. 2017; Kim 2023). However, the volcanic temperature signal is difficult to distinguish from other external forcings as well as internal climate variability when only examining one individual eruption (Fischer et al. 2007; Sjolte et al. 2021). Thus, a better assessment of how large eruptions affect Earth's climate and human societies must rely on a sample of large volcanic events.

Superposed epoch analysis (SEA) has been widely employed to decipher volcanic imprints in regional to global temperatures (Sear et al. 1987; Bradley 1988; Adams et al. 2003; Písek and Brázdil 2006; Esper et al. 2013; Gennaretti et al. 2014; Wilson et al. 2016; Neukom et al. 2018; Büntgen et al. 2020; Tejedor et al. 2021; Zhu et al. 2022). The core idea of SEA is to generate a composite response to a set of large volcanic eruptions by averaging out non-volcanic fluctuations (Haurwitz and Brier 1981). According to documented volcanic events and observed climate data since the beginning of the Industrial Era, large volcanic eruptions have been found to significantly cool global and hemispheric summer temperatures for 1–2 years (Sear et al. 1987; Bradley 1988; Robock and Mao 1995). However, these results are potentially biased by interference of the anthropogenic warming trend (Birkel et al. 2018) and by a small number of large eruptions in the observation period (Lough and Fritts 1987; Swingedouw et al. 2017).

High-resolution proxy records and climate model simulations have allowed extending the analysis of volcanic responses to times prior to the industrial period, when more large eruptions took place and anthropogenic impacts were less dominant (Schurer et al. 2013). Multiple lines of evidence from millennium-long datasets revealed that significant cooling by large volcanic eruptions (mainly tropical eruptions) lasted from five years to nearly a decade on the global and Northern Hemispheric scales (Schneider et al. 2017; Neukom et al. 2018; Tejedor et al. 2021), longer than inferred from instrumental data (Sear et al. 1987; Bradley 1988; Robock and Mao 1995). Yet, the magnitude and persistence of volcanic cooling is generally different between long-term reconstructions and simulations (e.g., Coupled Model Intercomparison Project 5-Paleoclimate Modelling Intercomparison Project Phase 3, (Schmidt et al. 2011); hereafter CMIP5-PMIP3 simulations) (Masson-Delmotte et al. 2013; Hartl-Meier et al. 2017; Neukom et al. 2018; Zhu et al. 2020). These discrepancies can be caused by seasonality and properties of different types of proxy data (Hartl-Meier et al. 2017; Neukom et al. 2018; Lücke et al. 2019; Zhu et al. 2020), model performance and configurations (Stevenson et al. 2017) as well as uncertainties in the

Accepted for publication in *Journal of Climate*. DOI 10.1175/JCLI-D-23-0107.1.

volcanic forcing used in simulations (Sigl et al. 2015; Jungclaus et al. 2017; Toohey and Sigl 2017; Dee and Steiger 2022).

Temperature-sensitive tree rings in cold environments are capable of precisely documenting large volcanic events (Hartl-Meier et al. 2017; Schneider et al. 2015; 2017), thus providing a unique opportunity to study volcanic cooling at annual resolution. Studies suggested that the data-model disagreements regarding large-scale volcanic responses can be reconciled by using maximum latewood density (MXD) of conifers growing in cold regions (Anchukaitis et al. 2012; Zhu et al. 2020), the most robust proxy due to superior temperature sensitivity and weak biological memory compared to other tree-ring parameters such as ring width (Björklund et al. 2019; Esper et al. 2015; Schneider et al. 2015; Wang et al. 2020). In recent years, several simulations of the last-millennium climate under the state-of-art Coupled Model Intercomparison Project 6-Paleoclimate Modelling Intercomparison Project Phase 4 protocol are now available (Jungclaus et al. 2017) (hereafter referred to as CMIP6-PMIP4 simulations), which use updated volcanic aerosol forcing compared to CMIP5-PMIP3. Comparing these new simulations with high-precision MXD data can better define the volcanic impacts and cooling mechanisms in the climate system.

However, volcanic cooling patterns revealed by tree-ring based climate reconstructions appear to be variable at sub-continental scales. For example, a cooling effect was significant for 1–2 years in Northern and Central Europe (Esper et al. 2013), Western United States (Heeter et al. 2021), and Tibetan Plateau (Duan et al. 2018), but extended for longer periods in Central Asia (Davi et al. 2021) and Eastern Canada (Gennaretti et al. 2014; Wang et al. 2022), especially after tropical eruptions. These regional differences could in part result from specific feedbacks due to local effects and circulation patterns (Písek and Brázdil 2006; Fischer et al. 2007; D'Arrigo et al. 2013; Guillet et al. 2017). On the other hand, the results can be sensitive to noise in proxy records (Christiansen and Ljungqvist 2017; Neukom et al. 2018), and selection of volcanic events (Rao et al. 2019; Zhu et al. 2022). Efforts have been made to take into account uncertainties related to eruption dates (Rao et al. 2019) and to investigate how biological memory affects volcanic signals recorded in tree-ring width data (Esper et al. 2015; Gennaretti et al. 2018; Lücke et al. 2019; Zhu et al. 2020). However, we should better understand how the precise detection of volcanic imprint at sub-continental scale is impacted by the selection of volcanic events, unforced climate variability, and proxy noise.

Accepted for publication in *Journal of Climate*. DOI 10.1175/JCLI-D-23-0107.1.

Circum-North Atlantic regions are an ideal test bed for addressing the above issues because they correspond to three main clusters of millennial temperature-sensitive MXD chronologies in the global tree-ring network (Esper et al. 2016; Wang et al. 2022) and both sides of the ocean appear to differ in the persistence of volcanic cooling in earlier studies (Esper et al. 2013; Gennaretti et al. 2014; Wang et al. 2022). In this paper, we thus revisit imprints of large explosive volcanism on land summer temperatures from three circum-North Atlantic regions during the last millennium, including Eastern Canada (ECan), and Northern and Central Europe (NEuro and CEuro). Our objectives are 1) to investigate factors (specific volcanic sensitivity, selection of eruptions, strength of unforced variability and proxy noise) that have potentially caused the variable volcanic responses of regional temperature reconstructions and 2) to assess the performance of the state-of-art CMIP6-PMIP4 simulations to account for volcanic responses. We first developed three millennial regional summer temperature reconstructions as a baseline to investigate how the detection of volcanic imprints is affected by the event selection. Subsequently, we performed a pseudoproxy experiment taking into account the internal climate variability and proxy noise embedded in the regional reconstructions. Lastly, we compared volcanic imprints in the reconstructions with those in five state-of-art CMIP6-PMIP4 millennial simulations, and discussed possible mechanisms of region-specific volcanic responses.

2. Methods

a. Summer temperature reconstructions

We developed three millennial land summer temperature reconstructions using available centennial-long MXD chronologies in ECan (4 sites), NEuro (6 sites), and CEuro (4 sites) (Fig. 1a, Table S1). As tree-ring data exhibit biological trends, standardization is needed to remove non-climatic variations from MXD measurements (Cook et al. 1990). By comparing three standardization methods (Wang et al. 2022; Table S2) including regional curve standardization (RCS; Briffa et al. 1992), signal-free RCS (Melvin and Briffa 2008), and the regionally constrained individual standardization (RSFi; Björklund et al. 2013), we finally applied the RSFi method in order to optimize temperature signals for chronologies from sites where raw MXD measurements are available (Table S1). For the remaining sites with unavailable raw MXD data for re-standardization, we directly used the chronologies standardized in the original studies, basically using RCS (Briffa et al. 1992). To be consistent with the published MXD chronologies, the RSFi

Accepted for publication in *Journal of Climate*. DOI 10.1175/JCLI-D-23-0107.1.

chronologies were calculated using residuals between power transformed MXD series (Cook and Peters 1997) and biological trends, and the Tukey's bi-weight robust mean. A detailed RSFi approach is described in (Wang et al. 2022). In fact, we found that volcanic signals in local chronologies (raw data available) are little affected by the choice of these RCS-based variants, which were developed to preserve long-term variability in tree-ring data (Supplementary Text S1).

Instrumental temperature targets for reconstructions were obtained from the CRU TS4.03 0.5º gridded monthly temperature dataset (Harris et al. 2020). We first calculated monthly regional temperatures by averaging data grids within three regions (land only), between 60–77ºW and 50–60ºN for ECan, 12–30ºE and 60–70ºN for NEuro, and 0–15ºE and 40–50ºN for CEuro (Fig. 1a). May to August (MJJA) mean temperatures of current year were chosen as the reconstruction target for each region because of optimal responses of the local MXD chronologies during this season (Fig. S1). The 1905–2000 common time period was used for calibrating most MXD chronologies, except for the Boniface (1905–1989 CE) and Lauenen (1905–1976 CE) sites in northern Quebec and the Swiss Alps due to limited data coverage, respectively. Reconstructions were developed using a linear Bayesian model which allows weighting the confidence of each model from individual MXD chronologies (Gennaretti et al. 2017). For each year, the final reconstructed temperature value was the median of the posterior distribution of the model output. The spatial domains of the three regional reconstructions were assessed by Pearson's correlation coefficients (hereafter Pearson's *r* or *r*) with 1º gridded MJJA temperatures (CRU TS4.03, HadISST v1.1 (Rayner et al. 2003), and the 20th Century Reanalysis v3) during 1905–2000 CE, and were only based on the 10-yr high-passed series to emphasize year-to-year coherence (Butterworth filter using the "dplR" R package; Bunn 2008). Statistical significance (i.e., *P* values) for correlations in this study were adjusted to account for autocorrelation of time series using the method of Hu et al. (2017).

b. Pseudoproxy experiment

To shed light on how strengths of unforced climate variability and proxy noise can affect volcanic imprints in climate reconstructions, we designed a pseudoproxy experiment only focusing on the response to tropical eruptions. The pseudoproxy experiment was based on the output of a 2D energy balance model (EBM) (Ziegler and Rehfeld 2021), which does not feature internal variability (Hegerl and Zwiers 2011). The employed EBM produces externally forced monthly

Accepted for publication in *Journal of Climate*. DOI 10.1175/JCLI-D-23-0107.1.

temperature variations on a T42 Gaussian (~2.8º) grid according to input radiative forcing and grid-specific heat capacity, albedo, thermal conductivity, and outgoing radiation. We first ran one full-forcing simulation for the 850–2000 CE period using time-varying solar, volcanic and greenhouse-gas forcings compiled by PAGES 2k Consortium (2019) and orbital parameters calculated from Berger (1978). We then generated regional MJJA temperatures from area-weighted means (land only) for the ECan, NEuro, and CEuro regions (Fig. 1a; Fig. S2a). The period 1000–1930 CE was retained for the subsequent pseudoproxy experiment to exclude the strong recent warming trend. We additionally ran a volcanic-only simulation forced by time-varying volcanic aerosols but with constant greenhouse gases (279 ppm), solar irradiation (1362 W m^{-2}), and orbital parameters to study potential temperature perturbations caused only by volcanic eruptions (but not used for the pseudoproxy experiment).

We then added unforced components to the full-forcing regional MJJA temperature series to produce "full" regional temperatures (hereafter "full" temperatures). According to the real-world estimations and climate model simulations showing low autocorrelation in the unforced temperature variability (Supplementary Text S2), it was represented by a random stochastic process (white noise) in ECan, NEuro, and CEuro. In each region we considered three scenarios, the LOW-unforced, MED-unforced and HIGH-unforced scenarios, where the ratios between standard deviations of unforced and fully forced MJJA temperatures were 0.5, 1, and 2 during 1000–1930 CE, respectively. Year-to-year variations of the regional unforced variability were set identical to ensure that only the amplitude would change among scenarios. Thus, we first generated one random white-noise time series with zero mean and unit variance and then adjusted its variance to form regional "full" temperatures in different scenarios. In total, we produced 100 sets of "full" temperatures per scenario in each region with different initial random white-noise time series (Figs. S2b–d).

Proxy noise was then added to one set of "full" temperatures randomly selected from the 100 sets produced above (Fig. S3). Proxy data are imperfect records of climate (Christiansen and Ljungqvist 2017) due to unexplained non-climatic variations (i.e., noise unrelated to the targeted reconstruction signal; Esper et al. 2015). The three MXD millennial temperature reconstructions showed relatively weak and similar autocorrelation structures (Fig. S4). Thus, we assumed that this proxy noise is a temporally stable white noise and that observational temperatures (CRU data) are noise free. For each region, we added noise with specific strength to the corresponding regional

Accepted for publication in *Journal of Climate*. DOI 10.1175/JCLI-D-23-0107.1.

"full" temperatures. The strength was set according to the correlation coefficient between the real-world MXD reconstruction and the May–August temperature target through signal-to-noise ratio (SNR) in each region (Smerdon 2012):

$$\mathrm{SNR} = \frac{\sigma_{\mathrm{full}}}{\sigma_{\mathrm{noise}}} = \sqrt{\frac{r^2}{1 - r^2}} \quad (1),$$

where σ_{full} and σ_{noise} denote standard deviations of the "full" temperature and proxy noise, respectively. Here we used the correlation (r) between the 10-year high-passed rather than the unfiltered MXD-based reconstruction and corresponding instrumental temperature target (1905–2000 CE) as the common warming trend in the unfiltered time series tends to downgrade the level of estimated noise. Finally, we generated a set of 100 pseudoproxy series per site and per scenario (Fig. S3). These pseudoproxy series were then calibrated against the corresponding regional "full" temperatures during 1000–1930 CE to mimic the necessary climate reconstruction process. Since each pseudo-reconstruction was based on a single pseudoproxy series, the linear-scaling approach (Esper et al. 2005), which forces the variances and means of the pseudoproxy series to equal that of the corresponding temperature target, is sufficient to produce results very similar to those using the above Bayesian method and was thus used for the calibration here.

c. CMIP6-PMIP4 climate model simulations

We used five CMIP6 millennial simulations of monthly near-surface temperature, sea-level pressure, and sea-ice concentration (Table 1) to investigate data-model agreement and potential mechanisms of region-specific volcanic responses. In general, each millennial simulation (CMIP6-PMIP4) consisted of a PMIP4 *past1000* or *past2k* run (Jungclaus et al. 2017) and the corresponding CMIP6 historical run to cover the entire last millennium (also see Supplementary Text S3). The CMIP6-PMIP4 *past1000* and *past2k* runs employed a state-of-art reconstruction of volcanic stratospheric sulfur injections based on synchronized bipolar ice cores before 1850 CE (i.e., the eVolv2k dataset), with dating uncertainty assumed to be smaller than ±2 years during the last 1500 years (Toohey and Sigl 2017), so their performance was expected to be better than CMIP5-PMIP3 simulations. All simulations were remapped to a T42 Gaussian grid using a conservative interpolation method provided by Climate Data Operators (Schulzweida 2019) and the monthly climate variables were aggregated to seasonal climate for each grid cell (MJJA and December–

Accepted for publication in *Journal of Climate*. DOI 10.1175/JCLI-D-23-0107.1.

February, DJF). We then generated simulated MJJA temperature series for ECan, NEuro, and CEuro using area-weighted mean.

Code	Model	Past + Historical experiment ID	Reference
CESM	CESM1	trans1-850AD	Zhong et al. (2018)
MIROC	MIROC-ES2L	r1i1p1f2 + r1i1000p1f2	Ohgaito et al. (2021)
MRI	MRI-ESM2.0	r1i1p1f1 + r1i1000p1f1	Yukimoto et al. (2019)
MPI0	MPI-ESM1-2-LR	run0 + r1i2000p1f1	van Dijk et al. (2022)
MPI1	MPI-ESM1-2-LR	r1i1p1f1 + r1i2000p1f1	van Dijk et al. (2022)

Table 1. CMIP6-PMIP4 millennial simulations used in this study.

d. Superposed epoch analysis (SEA)

SEA was used to investigate volcanic imprints in various climate time series (MXD reconstructions, chronologies, pseudo-reconstructions, simulations, and the 20th Century Reanalysis). We selected volcanic eruptions based on the stratospheric aerosol optical depth averaged between 30–90°N ($SAOD_{NHET}$) from the eVolv2k (Toohey and Sigl 2017) plus CMIP6 datasets, the same volcanic forcing as used in the EBM and CMIP6-PMIP4 simulations. While our previous study showed that a peak $SAOD_{NHET}$ value of 0.03 is a proper criterion for screening eruptions that potentially resulted in significant climate changes (Wang et al. 2022), here, we selected stronger events with peak $SAOD_{NHET} \geq 0.05$, roughly representing half of the magnitude of the 1991 Pinatubo eruption ($SAOD_{NHET}$ = 0.098). In total, 17 tropical and 12 Northern Hemisphere extratropical (NHET) eruptions between 1050 and 1960 CE were retained (hereafter referred to as SAOD events; Table S3). For SEAs on real-world time series (i.e., MXD chronologies, reconstructions, and reanalysis data), we accounted for a typical 1-year lag between unidentified tropical eruptions and sulfur depositions in ice cores according to the adjustment by Toohey et al. (2019), which can maximize the 3-year cooling in Northern Hemisphere temperature reconstructions. In contrast, the volcanic dates of the eVolv2k dataset were used for SEAs with pseudo-reconstructions and CMIP6-PMIP4 time series because these simulations were directly forced by the eVolv2k plus CMIP6 datasets. Though different eruption years were used for real-world and simulated climate, the same events were targeted. It is noteworthy that CMIP6-PMIP4 simulations assumed January as the eruption month for unidentified events in eVolv2k (Toohey

Accepted for publication in *Journal of Climate*. DOI 10.1175/JCLI-D-23-0107.1.

and Sigl 2017), which resulted in some data-model inconsistencies. A detailed SEA approach can be found in the Supplementary Text S4.

We additionally considered historic eruptions from the Global Volcano Program (2023) based only on a volcanic explosivity index (Newhall and Self 1982) ≥ 5 (hereafter the VEI events; Table S4) for SEA. The selected eruption events were only used to investigate how responses of the three reconstructions differ if we consider VEI events in place of SAOD events. VEI events are known to be less tightly related to climate forcing than ice-core-based events (Robock 2000), thus we used them to investigate the impact of potential uncertainties in the volcanic forcing.

We also carried out an experiment to study how the selection of volcanic events influences the result of SEA. First, *N* events were randomly sampled 100 times from the aforementioned SAOD eruptions without replacement, with *N* varying from 5–15 for tropical events. For NHET eruptions, *N* was set between five and nine so that more than 100 unique subsets can be randomly generated from a total number of 12 events. In each iteration, the selected *N* events were used in the SEA algorithm. In addition to the random resampling approach, we included only the largest *N* (same range as the above experiment) events for each type of eruption to account for a more common way to screen events for SEA.

3. Results

a. MXD-based reconstructions

The three MXD-based summer temperature reconstructions are highly and significantly correlated to regional MJJA mean temperatures (1905–2000 CE) and thus capture a large fraction of MJJA temperature variances in ECan (49%), NEuro (59%), and CEuro (40%), respectively. For each reconstruction, moving correlations with temperature targets in a 31-year window are significant ($P < 0.05$) through time since 1901 CE, with some variability in strength (Fig. S5). Although the three regional reconstructions show similar long-term warm and cold epochs during the last millennium, the year-to-year variance is the strongest in ECan, followed by NEuro and then CEuro (Fig. 1b). The CEuro reconstruction shows the lowest correlation between high-frequency (10-year high-passed) data and CRU temperatures (Fig. 1b), suggesting a higher level of non-temperature noise in the high-frequency domain. Field correlations of reconstructions resemble those of the observational regional temperatures (both CRU plus HadISST, and 20th

Accepted for publication in *Journal of Climate*. DOI 10.1175/JCLI-D-23-0107.1.

Century Reanalysis) in ECan and NEuro, but the spatial domain of the CEuro reconstruction is much weaker compared to that of the observed regional mean temperature (Fig. 1c; Fig. S6).

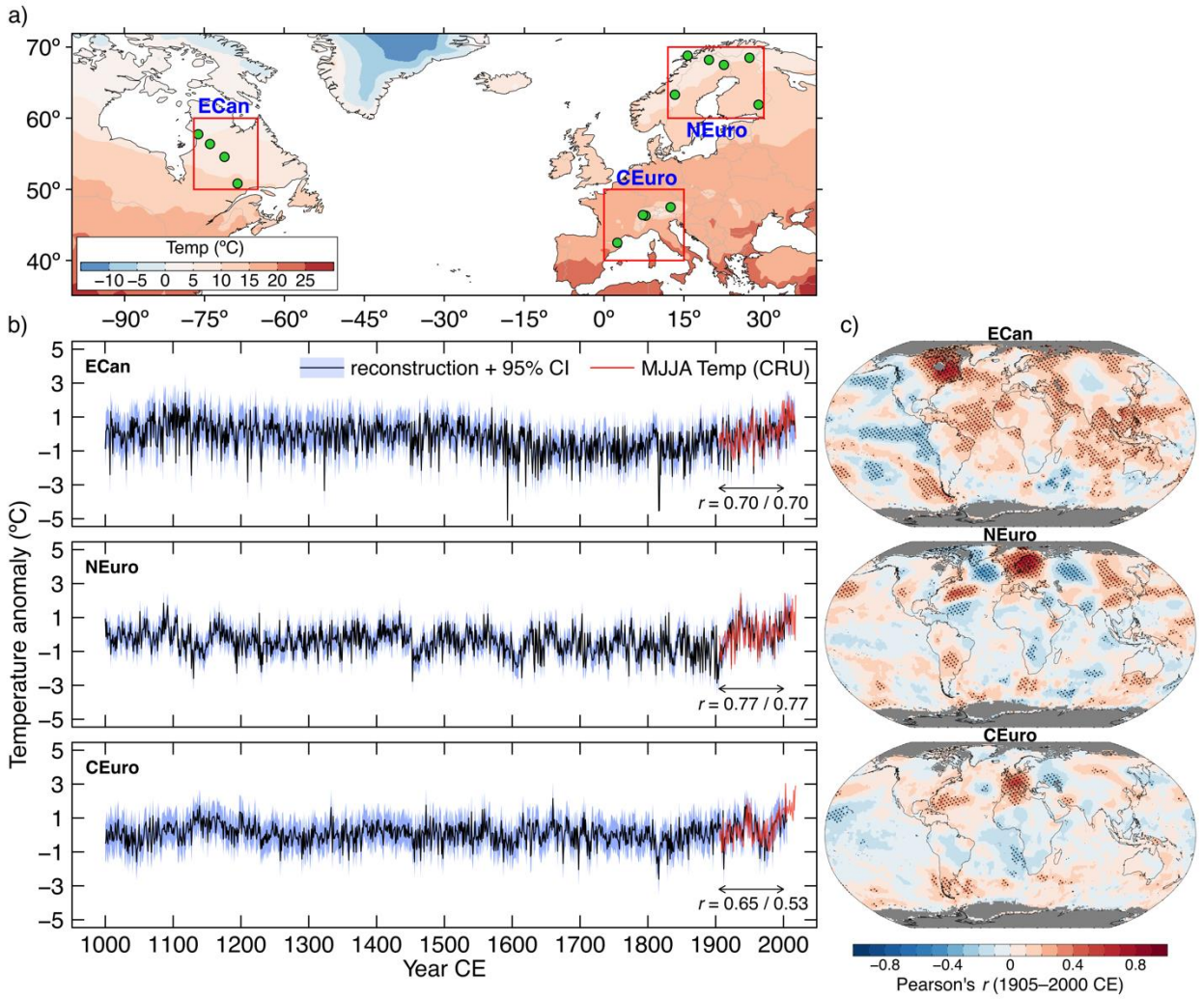

Fig. 1. Site map (a) and millennial density-based summer (May–August, MJJA) temperature reconstructions for the three circum-North Atlantic regions (b) as well as their field correlations (c) with observational MJJA temperatures (CRU plus HadISST datasets). In (a), rectangles encompass the areas used to calculate regional MJJA temperature targets over 1905–2000 CE (land only). Background colors show MJJA mean temperatures calculated from the CRU dataset. In each panel of (b), Pearson's *r* values are for raw reconstructions and regional temperature targets during the 1905–2000 period and 10-year high-passed series, orderly. 95% CI: the 95% confidence interval of Bayesian reconstructions. All temperature series are transformed to anomalies w.r.t. 1951–1980 CE. In (c), Pearson's *r* is based on 10-yr high-passed (Butterworth filter) data over 1905–2000 CE to avoid influence of long-term warming trend. Black dots: significant correlations ($P < 0.05$). Gray shading: Pearson's *r* unavailable due to missing values in the observational data.

b. Volcanic responses of regional reconstructions

Accepted for publication in *Journal of Climate*. DOI 10.1175/JCLI-D-23-0107.1.

SEAs based on eruptions with $SAOD_{NHET}$ values ≥ 0.05 reveal that large tropical eruptions resulted in more persistent significant summer cooling than NHET eruptions across the three circum-North Atlantic regions. In Eastern Canada, the reconstructed MJJA temperature dropped on average by 1.36ºC one year after tropical eruptions and persisted around −0.5ºC from year *t* + 2 until the 9th post-eruption year (Fig. 2a). Volcanic cooling in Europe is not as prominent as in ECan (−0.78ºC and −0.39ºC at the year *t* + 1), and remained significant for 5 and 4 years in NEuro and CEuro, respectively, with a recovery to the pre-eruption level during a few additional years (Figs. 2b, c). In contrast, NHET eruptions only produced a short temperature decrease in ECan (−0.90ºC) and CEuro (−0.40ºC) at the year of eruption, and at the year *t* + 1 in NEuro (−0.39ºC) (Figs. 2e–g). SEAs on normalized reconstructions (Fig. S7; normalized to have the same mean and variance) further confirm that volcanic eruptions have induced stronger summer cooling in the northwestern than eastern North Atlantic side during the last millennium (Figs. 2d, h), a phenomenon unrelated to the fact that the variance is the largest in the ECan reconstruction (Fig. 1b).

Compared to SAOD events, VEI events tended to have less coherent results among the three regional reconstructions, especially in terms of the duration of cooling after tropical eruptions. As shown in Fig. 2 (light curves), the significant cooling impacts are also generally weaker after both tropical and NHET volcanic eruptions.

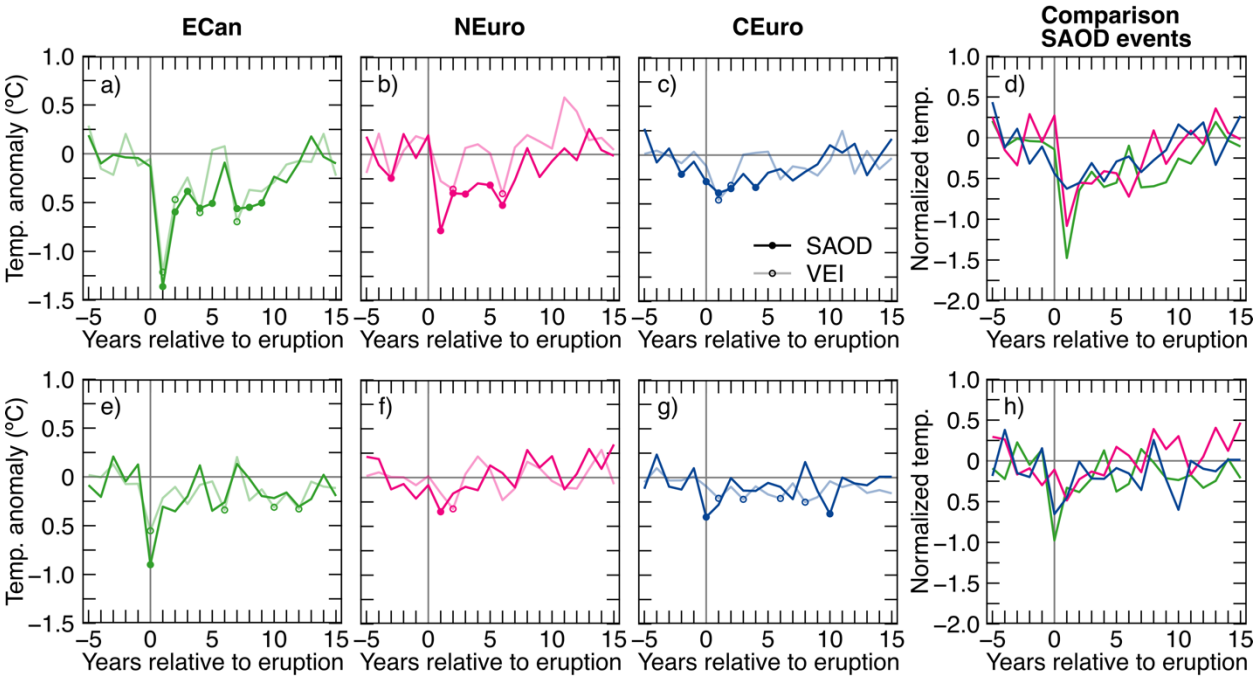

Accepted for publication in *Journal of Climate*. DOI 10.1175/JCLI-D-23-0107.1.

Fig. 2. Responses of the last-millennium reconstructed regional May–August temperatures to tropical (a–c) and NHET (e–g) volcanic eruptions. In (a)–(c) and (e)–(g) responses to SAOD and VEI events are shown in dark and light colors, respectively, with solid and open points indicating significant cooling ($\alpha = 0.05$; see Supplementary Text S4). In (d) and (h), only responses to SAOD events are presented, and the responses are based on normalized temperatures (z-scores relative to the 1000–2000 period; Fig. S7) in order to avoid the influence of region-specific temperature variance.

SEAs using subsets of SAOD tropical events indicate that the duration of significant cooling detected from the three MXD-based temperature reconstructions lengthens with the number of eruptions included in the analysis (Figs. 3a–c). Although these trends can be partially related to the fact that the bootstrapped confidence intervals shrink with a greater *N*, a similar result was observed if highlighting the first post-eruption year when the temperature anomalies exceeded the pre-eruption level (Figs. S8a–c), a method independent of the significance test. Moreover, smaller *N* generally resulted in less persistent cooling after tropical eruptions even if the largest events were targeted, despite larger events resulted in a stronger cooling peak in the composite response (Fig. S9). These results underscore the impact of number of selected events on the detection of volcanic cooling signal. In addition, for a given number of events, the cooling effect tends to last longer in ECan as compared to the two reconstructions from the eastern North Atlantic area (Figs. 3a–c). The effect of *N* on the cooling persistence is less evident following NHET eruptions (Figs. 3d–f; Figs. S8d–f, S9) since the cooling is ephemeral in nature and the average forcing is relatively weak (Table S3).

Accepted for publication in *Journal of Climate*. DOI 10.1175/JCLI-D-23-0107.1.

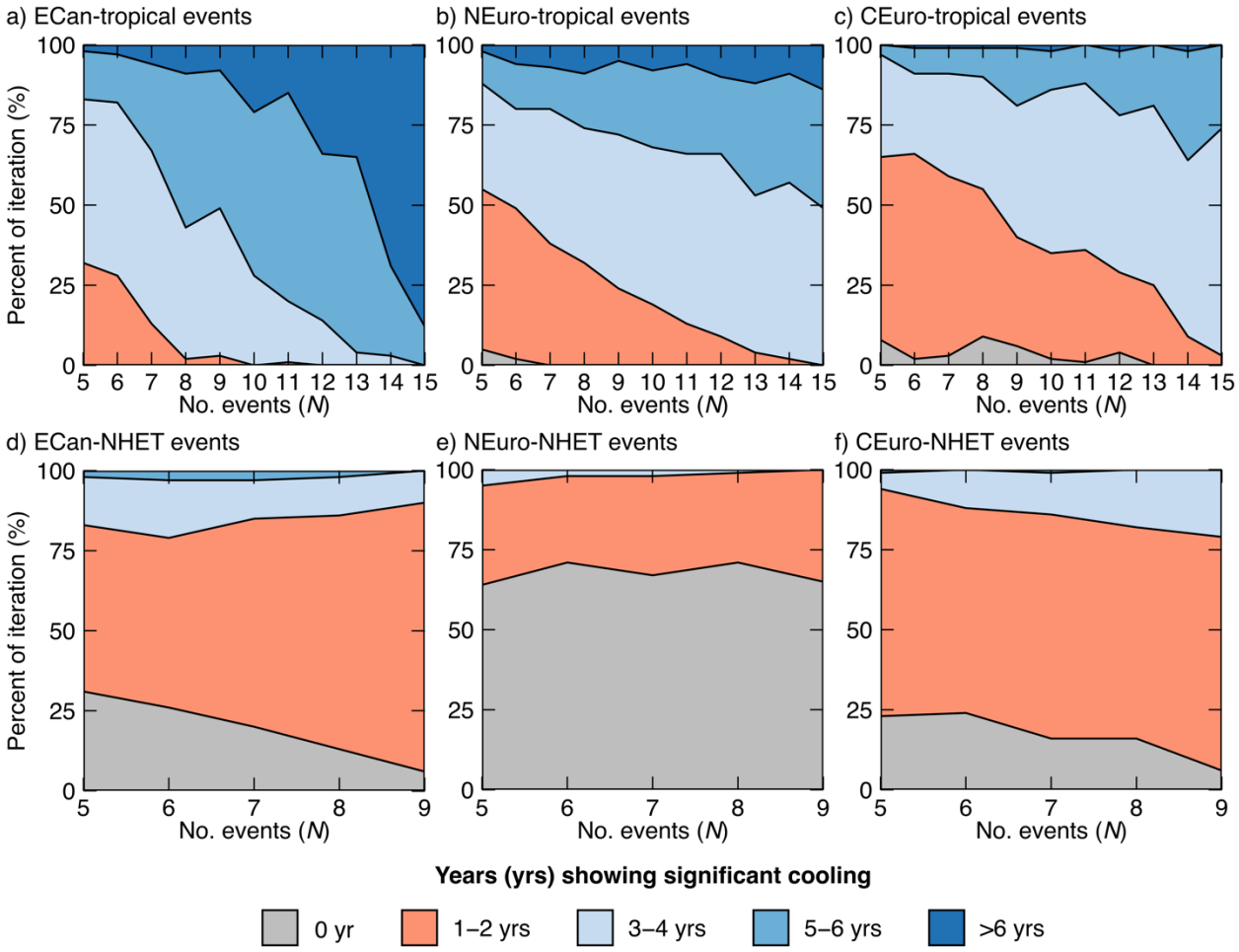

Fig.3. Years of significant cooling ($\alpha = 0.05$) according to the number of selected SAOD events (N) in SEAs. Volcanic events were randomly sampled 100 times without replacement from the full event list of each eruption type.

c. Effect of unforced variability and proxy noise

In the pseudoproxy experiment, we find that unforced temperature variability alters the apparent persistence of volcanic cooling and its magnitude. Although the shapes of the composite volcanic responses for "full" temperatures are similar among the three scenarios (LOW-unforced, MED-unforced and HIGH-unforced, see Methods), time periods of significant cooling become shorter with increasing unforced variability (Fig. 4; Fig. S10), due to the widening confidence interval of the significance test. The cooling peak (at year $t + 1$) of the "full" temperatures selected for the proxy noise experiment remains little changed from the LOW-unforced to HIGH-unforced scenario (Fig. 4). However, this pattern depends strongly on the overall effect of unforced variability. The 100 sets of "full" temperatures show that the cooling peak can increase, decrease

Accepted for publication in *Journal of Climate*. DOI 10.1175/JCLI-D-23-0107.1.

or remain unchanged with the strengthening unforced variability (Fig. S10), suggesting the importance of the local feedback mechanism in response to volcanic eruptions.

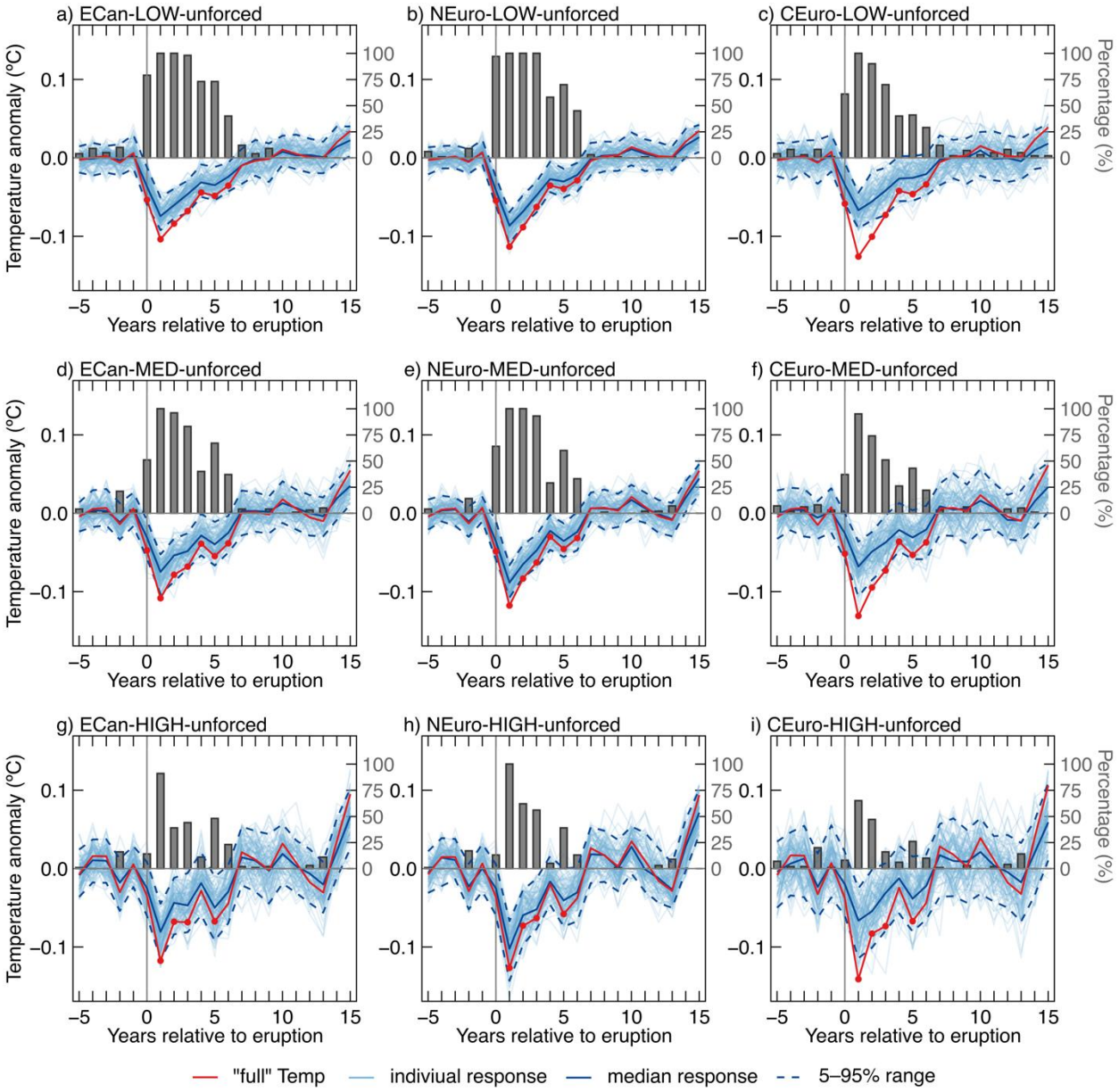

Fig. 4. Superposed epoch analyses of pseudoproxy series. Bars summarize the percentage of significant cooling (α = 0.05) out of 100 pseudo-reconstruction series (thin blue curves) in each year. Red points indicate significant cooling years (α = 0.05) for "full" temperatures (red curve). Note that the cooling magnitude of pseudoproxy series differs from that of the density-based reconstructions and CMIP6-PMIP4 simulations.

In contrast, proxy noise can substantially degrade volcanic cooling through climate reconstruction approaches. For the three scenarios, the peak cooling was on average decreased by ~30% and ~25% in ECan and NEuro, respectively (Fig. 4). In CEuro the median cooling reduced

Accepted for publication in *Journal of Climate*. DOI 10.1175/JCLI-D-23-0107.1.

by as much as ~50% relative to that of the corresponding "full" temperatures due to the largest amount of proxy noise (section 2b). Furthermore, the cooling ($P < 0.05$) in pseudo-reconstructions was less persistent. For the LOW-unforced scenario, about half of the pseudo-reconstructions showed a significant cooling for only 4 years or less in CEuro, compared to a 7-year significant cooling revealed by the "full" temperatures (Fig. 4c). More than 25% of the HIGH-unforced scenario in CEuro pseudo-reconstructions did not show any significant cooling, representing the most distorted case (Fig. 4i). This is because both strong unforced variability and proxy noise have muted the volcanic signal (degradation of the signal and of the power of the statistical test), even if the volcanic imprints persist in these synthetic pseudo-reconstruction time series.

d. Data-model comparison

The timing of the post-eruption cooling peak often differed by ± 1 year between CMIP6-PMIP4 simulations and MXD-based reconstructions (Figs. S11, S12). These inconsistencies can be related to the variability in model realizations and initial conditions, along with the fact that January was assigned as the eruption month for unidentified events in the CMIP6-PMIP4 volcanic forcing. However, the magnitude and duration of significant cooling following tropical eruptions agreed almost perfectly between the multimodel mean and temperature reconstructions in ECan and NEuro (Figs. 5a, b). The regional multimodel mean simulations are also consistent with the reconstructions in regard to the stronger temperature response in Eastern Canada compared to Europe (Figs. 5a–c). By contrast, the reconstruction displayed a much weaker peak volcanic response compared to simulations in CEuro (a cooling peak of −0.39ºC versus ~−0.80ºC, and 4-year versus ~10-year significant cooling; Fig. 5c). This mismatch most likely resulted from a large amount of proxy noise in the CEuro reconstruction as shown by our pseudoproxy experiment (see above).

Similar to MXD-based reconstructions, CMIP6-PMIP4 simulations displayed shorter cooling episodes after the sampled NHET eruptions compared to tropical eruptions (Fig. 5). However, individual simulations diverged significantly from reconstructions in their responses to NHET eruptions. For example, compared to a typical 1-year significant cooling in reconstructions, the MIROC simulation did not produce any significant cooling during summers in the three regions after major NHET eruptions, and some simulations produced a longer significant cooling ($P <$

Accepted for publication in *Journal of Climate*. DOI 10.1175/JCLI-D-23-0107.1.

0.05) in CEuro (Figs. 5d–f). Furthermore, after NHET eruptions, the multimodel mean disagreed with the reconstructions on the timing and magnitude of cooling peaks in ECan and NEuro, and the cooling in ECan is not stronger than that in Europe as suggested by the reconstructions. The multimodel mean's agreement with the reconstruction in CEuro may not imply a "perfect" data-model consistency given that the CEuro reconstruction is potentially affected by very strong proxy noise. Our results thus suggest that the CMIP6-PMIP4 models used in this study might have poorer performance in producing summer cooling after NHET than tropical eruptions and that the proxy network in CEuro should be improved.

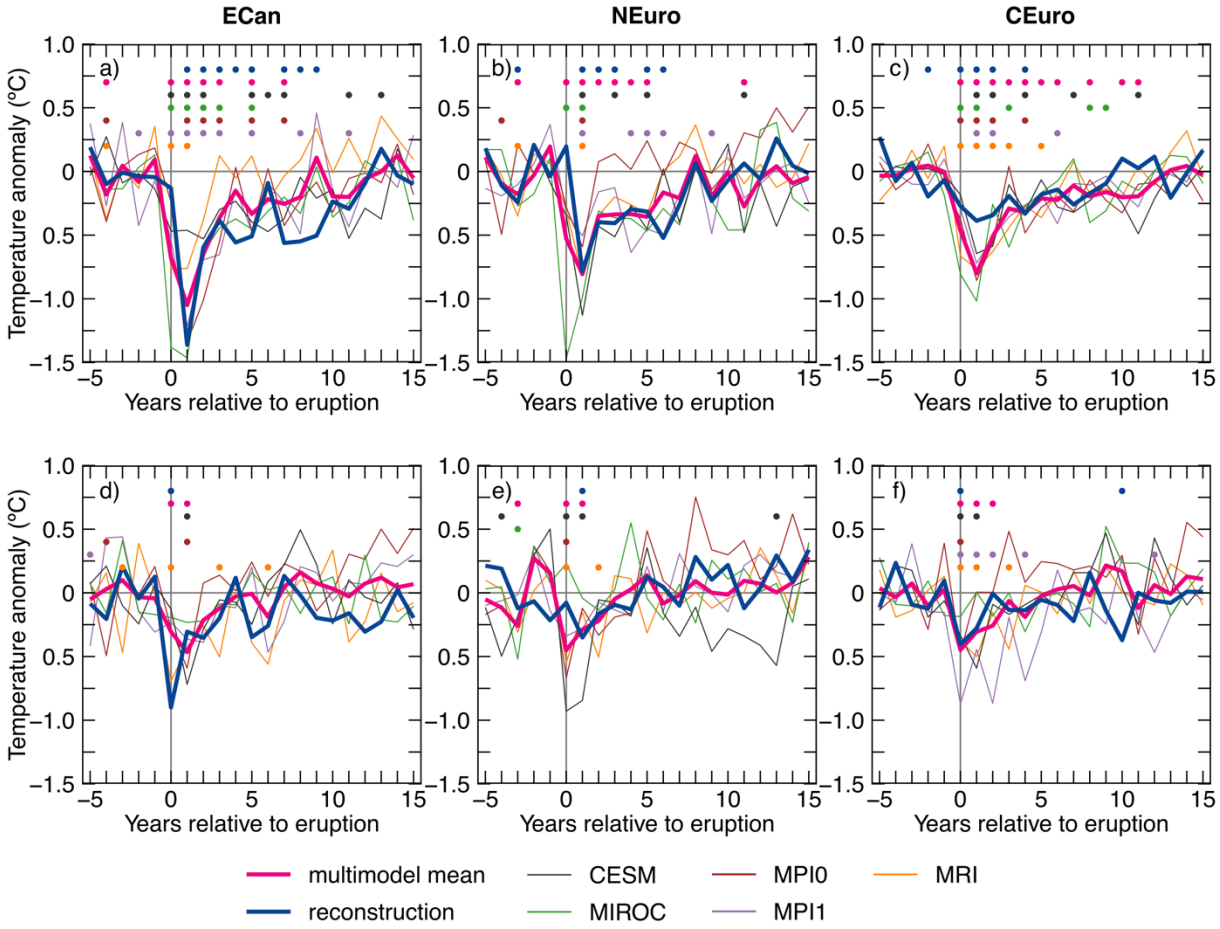

Fig. 5. Responses of the last-millennium reconstructed and CMIP6-PMIP4 simulated regional MJJA temperatures to tropical (a–c) and NHET (d–f) volcanic eruptions (SAOD events). Colored points indicate significant cooling years (α = 0.05) detected from corresponding temperature series.

4. Discussion

a. Revised volcanic responses and factors affecting detection of volcanic imprints

Accepted for publication in *Journal of Climate*. DOI 10.1175/JCLI-D-23-0107.1.

In this study, we found that tropical eruptions with large stratospheric sulfur injections induced prominent summer cooling for multiple years in northeastern North America, as well as in Europe, where pulse-like volcanic cooling was previously reported (Esper et al. 2013). In contrast, cooling caused by NHET eruptions was only significant for one year in the three regions because their aerosols mostly propagate in the Northern Hemisphere with a larger land mass that responds more rapidly to radiative forcing than ocean (Wang et al. 2022) and their average forcing is weaker than tropical eruptions (Table S3). These results are well reproduced by CMIP6-PMIP4 simulations (Fig. 5), suggesting they are robust. Results from the volcano-only EBM simulation (Figs. S13a–c), which excluded the effects of other forcing agents and internal climate variability, further indicates that the more persistent cooling caused by tropical eruptions is directly related to the Earth's energy balance, rather than a result due to closely spaced events (Figs. S13d–f). Consequently, the consistent regional volcanic responses highlight that tropical eruptions have the potential to shape multi-year temperature variations (Wang et al. 2022) and cause multi-year impacts on ecosystems (Gennaretti et al. 2018) and human society (Büntgen et al. 2020) in a vast region surrounding the North Atlantic Ocean.

However, several important factors need to be carefully considered to ensure the robustness of SEA when investigating imprints of explosive volcanic eruptions. First, volcanic events must be selected from informative data sources. The eVolv2k volcanic dataset identified from bipolar ice-core records (Toohey and Sigl 2017) has already allowed for an improved investigation of volcanic impacts, because ice-core volcanic index is directly related to stratospheric sulfur that drives Earth's climate variability (Robock 2000; Sigl et al. 2015). Conversely, the VEI scores are less directly associated with climate impacts (Newhall and Self 1982; Schmidt and Black 2022). The observation of the 1980 CE eruption of Mount St. Helens (VEI = 5) demonstrated that a large VEI does not necessarily corresponds to massive stratospheric sulfurs injection (Robock 2000). Thus, it is not surprising to observe inconsistent and short-term volcanic responses in our three circum-North Atlantic regions (Fig. 2) when using events with VEI $\geq$ 5. SAOD rather than VEI should be used to screen events for investigation of volcanic impacts on the climate system.

Second, the number and combination of volcanic events plays a critical role in SEA results as suggested by Zhu et al. (2022). Apparent volcanic responses were strongly dependent on the selected events when the number of events is small. Sufficient number of volcanic events can maximize the volcanic signal (Fischer et al. 2007; Swingedouw et al. 2017) and result in a less

Accepted for publication in *Journal of Climate*. DOI 10.1175/JCLI-D-23-0107.1.

biased composite response, especially regarding the cooling persistence of tropical eruptions (Figs. 3a–c). The resampling experiment suggested that the probability to detect a reliable volcanic response is higher than 50% when more than 10 large events are used for SEA (Fig. 3). On the other hand, the magnitude of events included in SEA should be large enough to induce regional to large-scale climate changes. Although multiple SAOD criteria have been used in different studies (Rao et al. 2019; Higgins et al. 2022), a peak SAOD value greater than 0.03 or 0.05 appears to be a suitable criterion to account for both forcing magnitude and number of events for a more robust SEA detection according to our experiments in the circum-North Atlantic regions (this study and Wang et al. 2022). In addition, mixing tropical and NHET eruptions potentially biases the understanding of cooling behaviors for specific eruption types. Combining a small proportion of NHET events with tropical events might lead to a changed response from which the cooling effect of NHET events can be misinterpreted (Wilson et al. 2016). Similar caution is needed for volcanic eruptions from the extratropical Southern Hemisphere, whose cooling behavior is poorly known due to the lack of long and robust proxy records (Neukom et al. 2014; Higgins et al. 2022).

Third, volcanic cooling can be underestimated due to inevitable noise in proxy records (Christiansen and Ljungqvist 2017; Neukom et al. 2018). The phenomenon is a direct result of the necessary reconstruction approach that "scales" proxy data (both noise and real climate) relative to climate observations (Lee et al. 2008). In fact, the "loss of variance" that would result from (ordinary least-square) regression-based reconstruction methods (Lee et al. 2008) has been partially mitigated by using the linear-scaling method for our pseudo-reconstructions. The volcanic cooling magnitude and duration can still be potentially reduced by as much as half in reconstructions with a correlation of 0.53 with the high-frequency domain of temperatures (i.e., CEuro in Fig. 4). Moreover, although a climate correlation of ~0.5 is a lower bound for MXD, it generally represents an average climate sensitivity for the more widely used tree-ring-width data (Anchukaitis et al. 2017). In addition, ring-width data include stronger biological memory that attenuates, lags, and extends apparent volcanic cooling over time (Esper et al. 2015; Lücke et al. 2019; Zhu et al. 2020). Thus, noisy ring-width data (Esper et al. 2015) and even MXD in regions where tree growth is less limited by temperatures are less suitable for studying volcanic effects.

At the same time, proxy noise exists in more complicated forms in the real world than our assumption of white noise. In tree-ring series, proxy noise can be time-varying (see Fig. S5 for time-varying temperature sensitivity) and introduced by various factors such as variable sample

Accepted for publication in *Journal of Climate*. DOI 10.1175/JCLI-D-23-0107.1.

replication, heterogenous sample types (Esper et al. 2016), disturbance during tree growth (Rydval et al. 2018), as well as tree-ring standardization (Helama et al. 2017) and reconstruction methods (Lee et al. 2008). Accordingly, individual proxy records may fail to accurately capture volcanic cooling even if they show a high correlation with climate during the calibration period, as shown by some local chronologies in CEuro and NEuro (see Fig. S14 and Table S1). In our study, local MXD chronologies are less strongly correlated with summer temperatures than the regional reconstructions (Table S1; Fig 1b) and they showed variable responses even within the same region (Fig. S14). The highly diverse volcanic responses in CEuro also indicated that the noise can be related to species-specific effects (e.g., larch budmoth frequently affected MXD of larch at the site Lots over the last millennium, Esper et al. 2007), seasonality (Fig. S1), as well as spatial representation of proxy (most CEuro sites are from high-elevation Alps and Pyrenees). All these factors have contributed to the strongly biased volcanic responses in the CEuro reconstruction, which was actually calibrated using temperatures covering a large spatial domain (Methods). Currently, proxy noise issues in the CEuro reconstruction have hampered a straightforward assessment of regional volcanic imprints in spite of the relatively consistent responses to tropical eruptions among CMIP6-PMIP4 simulations (Fig. 5c). Incorporating multiple high-quality proxy series unaffected by insect and fire disturbances with improved spatial coverage would offer a feasible way to further mitigate the proxy noise and thus lead to a more robust understanding of volcanic impact on the regional scale, such as in CEuro.

In addition, the significance of SEA is reduced by unforced variability, a major component of the Earth's climate variability that occurs on all spatial and temporal scales (Hegerl et al. 2007). As a non-volcanic "noise", unforced variability can dilute the volcanic signal, reduce the statistical power of SEA to identify significant cooling, and even alter the cooling magnitude depending on feedback mechanism of local climate in response to eruptions. Because unforced variability is much stronger on the regional than hemispheric scale (Fig. S15), extracting unbiased volcanic imprints from regional climate reconstructions with both strong unforced variability and proxy noise is a great challenge.

b. Performance of CMIP6-PMIP4 models

Climate system responses to volcanic eruptions can be further studied comparing simulations of general circulation models (GCMs) and proxy-based reconstructions, yet the performance of

Accepted for publication in *Journal of Climate*. DOI 10.1175/JCLI-D-23-0107.1.

GCM simulations needs to be evaluated. According to our results, the mean of the five simulations adequately reproduced the average response of summer temperatures to large tropical eruptions in the three circum-North Atlantic regions (Figs. 5a–c), though the lack of precise eruption month for unidentified events is a potential bias as eruption season can affect the responses of climate models (Toohey et al. 2011, 2019; Stevenson et al. 2017; Zhuo et al. 2021). On the other hand, regional responses tend to vary among individual simulations (Figs. 5a–c), despite the agreement on the hemispheric scale (Fig. S16a). This, along with inconsistent timing of cooling for single eruptions (Figs. S11, S12), indicates that the simulated unforced (internal) variability depends highly on the CMIP6 model (Table 1) (Pausata et al. 2015, 2016; Zanchettin et al. 2022). Ensemble simulations from multiple GCMs and multiple simulations per model are needed to study climate responses to volcanic eruptions, particularly when investigating regional scales (Pausata et al. 2015; Sjolte et al. 2021).

In contrast, the CMIP6-PMIP4 models appear to be less capable of simulating the response to NHET eruptions on regional scales (Figs. 5d–f). Even at the hemispheric scale, individual CMIP6-PMIP4 simulations show less consistent responses to NHET than to tropical eruptions (Fig. S16). This relatively poor performance may in part stem from large uncertainties in the reconstruction of volcanic aerosols after NHET eruptions, since the general rules for extratropical eruptions are not well understood (Crowley and Unterman 2013). First, unlike reconstructions of volcanic forcing for tropical eruptions having transfer functions based on a nuclear bomb test and Pinatubo observations (1991 CE), the transfer functions for extratropical events have frequently relied on model simulations of the Laki (1783 CE) and Novarupta (1912 CE) eruptions due to a lack of observations (Gao et al. 2007). Second, estimating the forcing of Icelandic eruptions is problematic because a large proportion of sulfate flux recorded in Greenland ice cores came from the troposphere rather than the stratosphere (Crowley and Unterman 2013; Toohey and Sigl 2017). Third, the simulated aerosol properties and forcing of NHET eruptions are strongly dependent on the eruption season and sulfur injection height (Toohey et al. 2019). The much weaker simulated than reconstructed cooling in ECan further suggests that the CMIP6-PMIP4 volcanic forcing for extratropical eruptions does not appear to be a strong overestimate, a result contrary to a model study (Aubry et al. 2020). More precise reconstructions of volcanic forcing for extratropical eruptions would be needed to better study how GCMs respond to different types of volcanic eruptions.

Accepted for publication in *Journal of Climate*. DOI 10.1175/JCLI-D-23-0107.1.

c. Why is Eastern Canada more sensitive to large volcanic eruptions?

Our data-model comparison additionally reveals that large tropical eruptions on average have a more pronounced cooling effect on the western than the eastern North Atlantic regions, a pattern in line with the 20th Century Reanalysis (Fig. S17) and the EKF400 paleo-reanalysis (Brönnimann et al. 2019). The SEAs based on gridded and normalized multimodel mean (Fig. S18) also confirm that this phenomenon is related neither to different areas used to produce three regional averages (Methods) nor to the different variances of regional temperatures series. To investigate what could have caused a stronger summer cooling in ECan, we compared region-specific volcanic response of the five CMIP6-PMIP4 and the full-forcing EBM simulations, concentrating on the maximum cooling at the year $t + 1$. The EBM simulation showed that the volcanic forcing alone is insufficient to induce a stronger cooling in ECan than in NEuro and CEuro (Fig. S19), although the EBM only accounts for a simplified radiation budget (Hegerl and Zwiers 2011; Ziegler and Rehfeld 2021). This points out that some positive feedback after large tropical eruptions most likely enhanced the summer cooling in the western North Atlantic region.

In fact, three out of the five CMIP6-PMIP4 simulations captured extremely cold episodes in ECan one year after tropical eruptions (MIROC, MPI0, and MPI1; see Fig. S19), all associated with a significant increase in sea-ice cover over the Labrador Sea and Hudson Bay regions during May–July (the left panel in Fig. 6). Sea ice growth in these regions can increase the average albedo (Ziegler and Rehfeld 2021), reflecting more solar radiation into space and thus cooling down regional temperatures. Post-eruption summers in ECan can be further cooled by potential atmosphere-ocean heat exchange with colder-than-normal sea waters surrounding the Quebec-Labrador Peninsula (see strong correlations between MJJA temperatures in ECan and the adjacent seas in Fig. S6).

According to the MIROC and MPI0 simulations, the anomalous May–July sea-ice growth and enhanced summer cooling in the eastern Canadian subarctic are most likely associated with intensified sea ice near Quebec-Labrador and the positive Arctic Oscillation (AO) and the North Atlantic Oscillation (NAO) in the first winter after tropical eruptions (Figs. 6c, d). During the positive winter NAO, representing lower sea-level pressure near Iceland and higher-than-normal pressure near the Azores Islands, cold conditions with more sea ice can occur across Eastern Canada (Figs. 6c, d; Wallace and Gutzler 1981; Boucher et al. 2017). Thus, more sea ice is

Accepted for publication in *Journal of Climate*. DOI 10.1175/JCLI-D-23-0107.1.

expected to remain until the next summer which further cools temperatures in this region (an additive effect to the cooling directly forced by volcanic aerosols). Although the positive NAO is also in conjunction with warmer-than-normal winter in Northern Eurasia (Wallace and Gutzler 1981; Fischer et al. 2007), the surrounding winter and summer sea ice is not decreased significantly after tropical eruptions in most CMIP6-PMIP4 simulations (Fig. 6). This suggests that the stronger cooling in ECan is less likely due to the damped summer cooling in Europe. Indeed, the NAO feedback mechanism is consistent with multiple lines of evidence from instrumental and reanalysis data (Fig. S17) (Mysak et al. 1996; Robock 2000; Christiansen 2008; Wunderlich and Mitchell 2017), climate reconstructions (Fischer et al. 2007; Ortega et al. 2015; Sjolte et al. 2021), and model studies (Zambri and Robock 2016; Swingedouw et al. 2017; Paik and Min 2018), which reported the intensification of polar vortex and the occurrence of positive NAO after large volcanic eruptions (Robock and Mao 1995; Robock 2000). Notably, the MRI simulation also produced a weak positive AO- and NAO-like structure (Fig. 6b). However, the associated winter cooling around Quebec-Labrador is not significantly colder than non-eruption years and the summer cooling is not stronger in ECan than in Europe in this simulation (Fig. S19).

Our analyses also underline that not all the five CMIP6-PMIP4 simulations produced consistent dynamical responses such as the positive winter AO and NAO. A particular interest regarding the model-specific response comes from the MPI0 and MPI1 runs (Figs. 6d, e) from the same model (van Dijk et al. 2022). Although both simulations showed stronger summer cooling along with sea ice growth in Eastern Canada than Europe after tropical eruptions, they displayed different NAO patterns, again suggesting the potential role of variable initial conditions and modelled unforced variability for GCM simulations.

Contrary to tropical eruptions, a recent study revealed that NHET ones can induce a negative phase of NAO in post-eruption winters and summers (Sjolte et al. 2021). Applying these assumptions to our study, then the summers in Eastern Canada may not be more sensitive to NHET eruptions than in Europe. However, we did observe contrarily a more pronounced cooling in the ECan reconstruction, although the CMIP6-PMIP4 simulations did not capture this feature (Figs. 5d–f). More robust proxy and model evidence is needed to investigate region-specific response to NHET eruptions in the North Atlantic region.

Accepted for publication in *Journal of Climate*. DOI 10.1175/JCLI-D-23-0107.1.

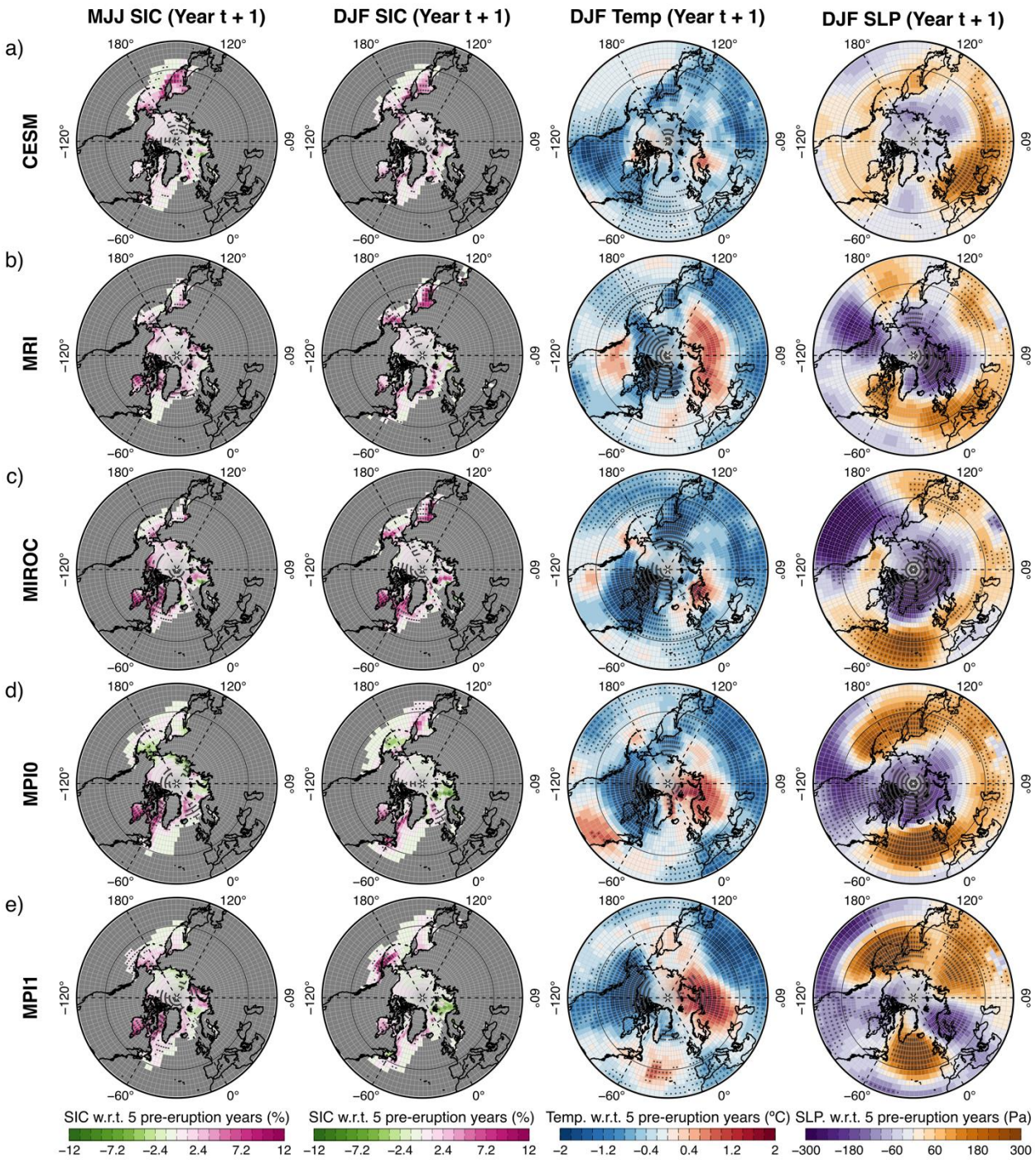

Fig. 6. SEA responses of CMIP6-PMIP4 simulated seasonal climate variables to tropical eruptions. Only the responses for Year t + 1 are shown. MJJ SIC: May–July sea-ice concentration; DJF SIC: December–February sea-ice concentration; DJF Temp: December–February surface air temperature at 2m; DJF SLP: December–February sea-level pressure. Note the January was set the reference year for the DJF variables. Thus, DJF shown here is the season before the MJJ season. The black dots indicate significant changes (α = 0.1) compared to 5 pre-eruption years calculated using the random bootstrapping significance test (Supplementary Text S4). Gray shading: unavailable sea ice coverage.

Accepted for publication in *Journal of Climate*. DOI 10.1175/JCLI-D-23-0107.1.

5. Conclusion

This study re-examined the impacts of tropical and NHET eruptions on the last-millennium land summer temperatures in three regions surrounding the North Atlantic Ocean (ECan, NEuro, and CEuro). While confirming that strong tropical eruptions had a more persistent cooling impact, on average, than the relatively weaker NHET eruptions in all three regions, we emphasize that the results of SEA depend strongly on the selection of volcanic events as well as proxy noise, and unforced climate variability. Developing more high-quality, annually resolved proxy records covering a wide spatial domain, in particular, the highly temperature-sensitive MXD data, is still demanded to potentially mitigate proxy-related noise for a more accurate investigation of volcanic imprints, especially in regions with very strong unforced climate variability.

In this study, we also assessed for the first time the performance of the state-of-art CMIP6-PMIP4 models to simulate volcanic responses. These new last-millennium simulations have shown a good performance in reproducing the average response of summer temperatures to tropical eruptions on regional and hemispheric scales. But the skill to simulate the significant response to NHET eruptions is generally poorer in terms of both cooling magnitude and persistence, likely due to potential uncertainties in estimating the forcing of NHET eruptions, and model sensitivity. A more comprehensive assessment of the CMIP6-PMIP4 last-millennium simulations requires a larger ensemble, but its generation has lagged behind other CMIP6-PMIP4 experiments (see https://pcmdi.llnl.gov/CMIP6/ArchiveStatistics/esgf_data_holdings/PMIP/index.html). In addition, dating uncertainty in the volcanic forcing leads to some disagreement between simulations and the real-world proxy data. Efforts to improve dating precision in volcanic reconstructions may further improve model-proxy comparisons over the last millennium.

We also found that the western North Atlantic is the most sensitive to tropical eruptions among the three studied circum-North Atlantic regions. Tropical eruptions may have produced positive phases of AO and NAO and amplified the colder-than-normal conditions in the first post-eruption winter near Quebec-Labrador, associated with sea ice growth. Accordingly, volcanic cooling in the following summer can be sustained by the increased sea ice. It, however, remains a question whether NHET eruptions could also lead to a colder summer in western than eastern North Atlantic as suggested by the three regional MXD-based reconstructions.

Acknowledgements.

Accepted for publication in *Journal of Climate*. DOI 10.1175/JCLI-D-23-0107.1.

F.W. and P.F. received funding from the GEOTOP and the Discovery Grants program of Natural Sciences and Engineering Research Council of Canada (NSERC-Discovery Grant, RGPIN-2019-06593). D.A. was supported by the NSERC-Discovery Grant (RGPIN-2021-02692). É.B. was supported by the NSERC-Discovery Grant (RGPIN-2021-04216 and RGPIN-2016-05244). F.W., D.A., É.B., and P.F. were further supported by the NSERC in collaboration with Hydro-Québec, Manitoba Hydro, and Ouranos under the PERSISTENCE project (RDC 485475-2015). F.G. was supported by the NSERC-Discovery Grant (RGPIN-2021-03553) and by the Canadian Research Chair in dendroecology and dendroclimatology (CRC-2021-00368). S.Y. was supported by Science and Technology Department of the Xinjiang Autonomous Region (grants 2020D04040, 2018D04028). Authors acknowledge Matthew Toohey for reading through the initial manuscript and providing constructive comments, Johann Jungclaus for providing two MPI-ESM1-2-LR *past2k* simulations with explanations, and Dirk Olonscheck for his help with the gridded multimodel mean of eight single-model large ensembles (Olonscheck et al. 2021). Support for the Twentieth Century Reanalysis Project version 3 dataset is provided by the U.S. Department of Energy, Office of Science Biological and Environmental Research (BER), by the National Oceanic and Atmospheric Administration Climate Program Office, and by the NOAA Earth System Research Laboratory Physical Sciences Laboratory. The authors declare no conflicts of interest.

Data Availability Statement.

The three regional temperature reconstructions are available at World Data Service for Paleoclimatology, NOAA National Centers for Environmental Information (https://www.ncei.noaa.gov/access/paleo-search/study/38080). The R code used to perform analyses in this study can be obtained from the corresponding author upon request. Tree-ring density data used to produce the three reconstructions are available at https://www.ncei.noaa.gov/products/paleoclimatology. The CMIP6 simulations are available at https://esgf-node.llnl.gov/projects/cmip6/ (the MPI0 simulation was provided by Johann Jungclaus).

Accepted for publication in *Journal of Climate*. DOI 10.1175/JCLI-D-23-0107.1.

REFERENCES

Adams, J. B., M. E. Mann, and C. M. Ammann, 2003: Proxy evidence for an El Niño-like response to volcanic forcing. *Nature*, **426**, 274–278, https://doi.org/10.1038/nature02101.

Anchukaitis, K. J., and Coauthors, 2012: Tree rings and volcanic cooling. *Nat. Geosci.*, **5**, 836–837, https://doi.org/10.1038/ngeo1645.

——, and Coauthors, 2017: Last millennium Northern Hemisphere summer temperatures from tree rings: Part II, spatially resolved reconstructions. *Quat. Sci. Rev.*, **163**, 1–22, https://doi.org/10.1016/j.quascirev.2017.02.020.

Aubry, T. J., M. Toohey, L. Marshall, A. Schmidt, and A. M. Jellinek, 2020: A new volcanic stratospheric sulfate aerosol forcing emulator (EVA_H): Comparison with interactive stratospheric aerosol models. *J. Geophys. Res. Atmos.*, **125**, e2019JD031303, https://doi.org/10.1029/2019JD031303.

Berger, A. L., 1978: Long-term variations of daily insolation and Quaternary climatic changes. *J. Atmos. Sci.*, **35**, 2362–2367, https://doi.org/10.1175/1520-0469(1978)035<2362:LTVODI>2.0.CO;2.

Birkel, S. D., P. A. Mayewski, K. A. Maasch, A. V. Kurbatov, and B. Lyon, 2018: Evidence for a volcanic underpinning of the Atlantic multidecadal oscillation. *npj Clim. Atmos. Sci.*, **1**, 24, https://doi.org/10.1038/s41612-018-0036-6.

Björklund, J., and Coauthors, 2019: Scientific merits and analytical challenges of tree-ring densitometry. *Rev. Geophys.*, **57**, 1224–1264, https://doi.org/10.1029/2019RG000642.

——, B. E. Gunnarson, P. J. Krusic, H. Grudd, T. Josefsson, L. Östlund, and H. W. Linderholm, 2013: Advances towards improved low-frequency tree-ring reconstructions, using an updated *Pinus sylvestris* L. MXD network from the Scandinavian Mountains. *Theor. Appl. Climatol.*, **113**, 697–710, https://doi.org/10.1007/s00704-012-0787-7.

Boucher, É., A. Nicault, D. Arseneault, Y. Bégin, and M. P. Karami, 2017: Decadal variations in eastern Canada's taiga wood biomass production forced by ocean-atmosphere interactions. *Sci.Rep.*, **7**, 2457, https://doi.org/10.1038/s41598-017-02580-9.

Accepted for publication in *Journal of Climate*. DOI 10.1175/JCLI-D-23-0107.1.

Bradley, R. S., 1988: The explosive volcanic eruption signal in northern hemisphere continental temperature records. *Climatic Change*, **12**, 221–243, https://doi.org/10.1007/BF00139431.

Briffa, K. R., P. D. Jones, T. S. Bartholin, D. Eckstein, F. H. Schweingruber, W. Karlén, P. Zetterberg, and M. Eronen, 1992: Fennoscandian summers from AD 500: temperature changes on short and long timescales. *Climate Dyn.*, **7**, 111–119, https://doi.org/10.1007/BF00211153.

Brönnimann, S., and Coauthors, 2019: Last phase of the Little Ice Age forced by volcanic eruptions. *Nat. Geosci.*, **12**, 650–656, https://doi.org/10.1038/s41561-019-0402-y.

Bunn, A. G., 2008: A dendrochronology program library in R (dplR). *Dendrochronologia*, **26**, 115–124, https://doi.org/10.1016/j.dendro.2008.01.002.

Büntgen, U., and Coauthors, 2016: Cooling and societal change during the Late Antique Little Ice Age from 536 to around 660 AD. *Nat. Geosci.*, **9**, 231–236, https://doi.org/10.1038/ngeo2652.

——, and Coauthors, 2020: Prominent role of volcanism in Common Era climate variability and human history. *Dendrochronologia*, **64**, 125757, https://doi.org/10.1016/j.dendro.2020.125757.

Christiansen, B., 2008: Volcanic eruptions, large-scale modes in the Northern Hemisphere, and the El Niño–Southern Oscillation. *J. Climate*, **21**, 910–922, https://doi.org/10.1175/2007JCLI1657.1.

——, and F. C. Ljungqvist, 2017: Challenges and perspectives for large-scale temperature reconstructions of the past two millennia. *Rev. of Geophys.*, **55**, 40–96, https://doi.org/10.1002/2016RG000521.

Cook, E. R., K. Briffa, S. Shiyatov, and V. Mazepa, 1990: Tree-ring standardization and growth trend estimation. *Methods of Dendrochronology: applications in the environmental sciences*, E.R. Cook ER, and L.A. Kairiukstis Eds., Springer Science & Business Media, 104–122.

——, and K. Peters, 1997: Calculating unbiased tree-ring indices for the study of climatic and environmental change. *Holocene*, **7**, 361–370, https://doi.org/10.1177/095968369700700314.

Accepted for publication in *Journal of Climate*. DOI 10.1175/JCLI-D-23-0107.1.

Crowley, T. J., and M. B. Unterman, 2013: Technical details concerning development of a 1200 yr proxy index for global volcanism. *Earth Syst. Sci. Data*, **5**, 187–197, https://doi.org/10.5194/essd-5-187-2013.

D'Arrigo, R., R. Wilson, and K. J. Anchukaitis, 2013: Volcanic cooling signal in tree ring temperature records for the past millennium. *J. Geophys. Res. Atmos.*, **118**, 9000–9010, https://doi.org/10.1002/jgrd.50692.

Davi, N. K., and Coauthors, 2021: Accelerated recent warming and temperature variability over the past eight centuries in the central Asian Altai from blue Intensity in tree rings. *Geophys. Res. Lett.*, **48**, e2021GL092933, https://doi.org/10.1029/2021GL092933.

Dee, S. G., and N. J. Steiger, 2022: ENSO's response to volcanism in a data assimilation-based paleoclimate reconstruction over the Common Era. *Paleoceanogr. Paleoclimatol.*, **37**, e2021PA004290, https://doi.org/10.1029/2021PA004290.

van Dijk, E., J. Jungclaus, S. Lorenz, C. Timmreck, and K. Krüger, 2022: Was there a volcanic-induced long-lasting cooling over the Northern Hemisphere in the mid-6th–7th century? *Climate Past*, **18**, 1601–1623, https://doi.org/10.5194/cp-18-1601-2022.

Duan, J., and Coauthors, 2018: Summer cooling driven by large volcanic eruptions over the Tibetan Plateau. *J. Climate*, **31**, 9869–9879, https://doi.org/10.1175/JCLI-D-17-0664.1.

Esper, J., D. C. Frank, R. J. S. Wilson, and K. R. Briffa, 2005: Effect of scaling and regression on reconstructed temperature amplitude for the past millennium. *Geophys. Res. Lett.*, **32**, L07711, https://doi.org/10.1029/2004GL021236.

——, U. Büntgen, D.C. Frank, D. Nievergelt, and A. Liebhold, 2007: 1200 years of regular outbreaks in alpine insects. *Proc. Royal Soc. B*, **274**, 671–679, https://doi.org/10.1098/rspb.2006.0191.

——, L. Schneider, P. J. Krusic, J. Luterbacher, U. Büntgen, M. Timonen, F. Sirocko, and E. Zorita, 2013: European summer temperature response to annually dated volcanic eruptions over the past nine centuries. *Bull. Volcanol.*, **75**, 736, https://doi.org/10.1007/s00445-013-0736-z.

Accepted for publication in *Journal of Climate*. DOI 10.1175/JCLI-D-23-0107.1.

——, ——, J. E. Smerdon, B. R. Schöne, and U. Büntgen, 2015: Signals and memory in tree-ring width and density data. *Dendrochronologia*, **35**, 62–70, https://doi.org/10.1016/j.dendro.2015.07.001.

——, and Coauthors, 2016: Ranking of tree-ring based temperature reconstructions of the past millennium. *Quat. Sci. Rev.*, **145**, 134–151, https://doi.org/10.1016/j.quascirev.2016.05.009.

Fischer, E. M., J. Luterbacher, E. Zorita, S. F. B. Tett, C. Casty, and H. Wanner, 2007: European climate response to tropical volcanic eruptions over the last half millennium. *Geophys. Res. Lett.*, **34**, L05707, https://doi.org/10.1029/2006GL027992.

Gao, C., L. Oman, A. Robock, and G. L. Stenchikov, 2007: Atmospheric volcanic loading derived from bipolar ice cores: Accounting for the spatial distribution of volcanic deposition. *J. Geophys. Res. Atmos.*, **112**, D09109, https://doi.org/10.1029/2006JD007461.

——, Y. Gao, Q. Zhang, and C. Shi, 2017: Climatic aftermath of the 1815 Tambora Eruption in China. *J. Meteor. Res.*, **31**, 28–38, https://doi.org/10.1007/s13351-017-6091-9.

Gautier, E., and Coauthors, 2019: 2600-years of stratospheric volcanism through sulfate isotopes. *Nat. Commun.*, **10**, 466, https://doi.org/10.1038/s41467-019-08357-0.

Gennaretti, F., D. Arseneault, A. Nicault, L. Perreault, and Y. Bégin, 2014: Volcano-induced regime shifts in millennial tree-ring chronologies from northeastern North America. *Proc. Natl. Acad. Sci. USA*, **111**, 10077–10082, https://doi.org/10.1073/pnas.1324220111.

——, D. Huard, M. Naulier, M. Savard, C. Bégin, D. Arseneault, and J. Guiot, 2017: Bayesian multiproxy temperature reconstruction with black spruce ring widths and stable isotopes from the northern Quebec taiga. *Climate. Dyn.*, **49**, 4107–4119, https://doi.org/10.1007/s00382-017-3565-5.

——, and Coauthors, 2018: Underestimation of the Tambora effects in North American taiga ecosystems. *Environ. Res. Lett.*, **13**, 034017, https://doi.org/10.1088/1748-9326/aaac0c.

Global Volcanism Program, 2023: Volcanoes of the World, v. 5.0.4. Smithsonian Institution, compiled by Venzke, E, 17 Apr 2023, https://doi.org/10.5479/si.GVP.VOTW5-2022.5.0.

Guillet, S., and Coauthors, 2017: Climate response to the Samalas volcanic eruption in 1257 revealed by proxy records. *Nat. Geosci.*, **10**, 123–128, https://doi.org/10.1038/ngeo2875.

Accepted for publication in *Journal of Climate*. DOI 10.1175/JCLI-D-23-0107.1.

——, C. Corona, F. Ludlow, C. Oppenheimer, and M. Stoffel, 2020: Climatic and societal impacts of a "forgotten" cluster of volcanic eruptions in 1108-1110 CE. *Sci. Rep.*, **10**, 6715, https://doi.org/10.1038/s41598-020-63339-3.

Harington, C. R., 1992: *The year without a summer? : World Climate in 1816*. Canadian Museum of Nature, 576 pp.

Harris, I., T. J. Osborn, P. Jones, and D. Lister, 2020: Version 4 of the CRU TS monthly high-resolution gridded multivariate climate dataset. *Sci. Data*, **7**, 109, https://doi.org/10.1038/s41597-020-0453-3.

Hartl-Meier, C. T. M., U. Büntgen, J. E. Smerdon, E. Zorita, P. J. Krusic, F. C. Ljungqvist, L. Schneider, and J. Esper, 2017: Temperature covariance in tree ring reconstructions and model simulations over the past millennium. *Geophys. Res. Lett.*, **44**, 9458–9469, https://doi.org/10.1002/2017GL073239.

Haurwitz, M. W., and G. W. Brier, 1981: A critique of the superposed epoch analysis method: its application to solar–weather relations. *Mon. Wea. Rev.*, **109**, 2074–2079, https://doi.org/10.1175/1520-0493(1981)109<2074:ACOTSE>2.0.CO;2.

Heeter, K. J., M. L. Rochner, and G. L. Harley, 2021: Summer air temperature for the Greater Yellowstone ecoregion (770–2019 CE) over 1,250 years. *Geophys. Res. Lett.*, **48**, e2020GL092269, https://doi.org/10.1029/2020GL092269.

Hegerl, G., and F. Zwiers, 2011: Use of models in detection and attribution of climate change. *Wiley Interdiscip. Rev.: Climate Change*, **2**, 570–591, https://doi.org/10.1002/wcc.121.

——, and Coauthors, 2007: Understanding and attributing climate change. *IPCC, 2007: Climate Change 2007: The Physical Science Basis*, S. Solomon et al., Eds., Cambridge University Press, 663–746.

Helama, S., T. M. Melvin, and K. R. Briffa, 2017: Regional curve standardization: State of the art. *Holocene*, **27**, 172–177, https://doi.org/10.1177/0959683616652709.

Higgins, P. A., J. G. Palmer, C. S. M. Turney, M. S. Andersen, and F. Johnson, 2022: Do Southern Hemisphere tree rings record past volcanic events? A case study from New Zealand. *Climate Past*, **18**, 1169–1188, https://doi.org/10.5194/cp-18-1169-2022.

Accepted for publication in *Journal of Climate*. DOI 10.1175/JCLI-D-23-0107.1.

Hu, J., J. Emile-Geay, and J. Partin, 2017: Correlation-based interpretations of paleoclimate data–where statistics meet past climates. *Earth Planet. Sci. Lett.*, **459**, 362–371, https://doi.org/10.1016/j.epsl.2016.11.048.

Huhtamaa, H., M. Stoffel, and C. Corona, 2022: Recession or resilience? Long-range socioeconomic consequences of the 17th century volcanic eruptions in northern Fennoscandia, *Climate Past*, 18, 2077–2092, https://doi.org/10.5194/cp-18-2077-2022.

Jungclaus, J. H., and Coauthors, 2017: The PMIP4 contribution to CMIP6 – Part 3: The last millennium, scientific objective, and experimental design for the PMIP4 past1000 simulations. *Geosci. Model Dev.*, **10**, 4005–4033, https://doi.org/10.5194/gmd-10-4005-2017.

Kim, S., 2023: Successive volcanic eruptions (1809–1815) and two severe famines of Korea (1809–1810, 1814–1815) seen through historical records. *Climatic Change*, 176, 1, https://doi.org/10.1007/s10584-023-03480-w.

Lee, T. C. K., F. W. Zwiers, and M. Tsao, 2008: Evaluation of proxy-based millennial reconstruction methods. *Climate Dyn.*, **31**, 263–281, https://doi.org/10.1007/s00382-007-0351-9.

Lough, J. M., and H. C. Fritts, 1987: An assessment of the possible effects of volcanic eruptions on North American climate using tree-ring data, 1602 to 1900 A.D. *Climatic Change*, **10**, 219–239, https://doi.org/10.1007/BF00143903.

Lücke, L. J., G. C. Hegerl, A. P. Schurer, and R. Wilson, 2019: Effects of memory biases on variability of temperature reconstructions. *J. Climate*, **32**, 8713–8731, https://doi.org/10.1175/JCLI-D-19-0184.1.

Marshall, L. R., E. C. Maters, A. Schmidt, C. Timmreck, A. Robock, and M. Toohey, 2022: Volcanic effects on climate: recent advances and future avenues. *Bull. Volcanol.*, **84**, 54, https://doi.org/10.1007/s00445-022-01559-3.

Masson-Delmotte, V., and Coauthors, 2013: Information from Paleoclimate Archives. *Climate Change 2013: The Physical Science Basis*, T.F. Stocker et. al., Eds., Cambridge University Press, 383–464.

Accepted for publication in *Journal of Climate*. DOI 10.1175/JCLI-D-23-0107.1.

McConnell, J. R., and Coauthors, 2020: Extreme climate after massive eruption of Alaska's Okmok volcano in 43 BCE and effects on the late Roman Republic and Ptolemaic Kingdom. *Proc. Natl. Acad. Sci. USA*, **117**, 15443, https://doi.org/10.1073/pnas.2002722117.

Melvin, T. M., and K. R. Briffa, 2008: A "signal-free" approach to dendroclimatic standardisation. *Dendrochronologia*, **26**, 71–86, https://doi.org/10.1016/j.dendro.2007.12.001.

Mysak, L. A., R. G. Ingram, J. Wang, and A. van der Baaren, 1996: The anomalous sea- ice extent in Hudson bay, Baffin bay and the Labrador sea during three simultaneous NAO and ENSO episodes. *Atmos.-Ocean*, **34**, 313–343, https://doi.org/10.1080/07055900.1996.9649567.

Neukom, R., and Coauthors, 2014: Inter-hemispheric temperature variability over the past millennium. *Nat. Climate Change*, **4**, 362–367, https://doi.org/10.1038/nclimate2174.

——, A. P. Schurer, Nathan. J. Steiger, and G. C. Hegerl, 2018: Possible causes of data model discrepancy in the temperature history of the last millennium. *Sci. Rep.*, **8**, 7572, https://doi.org/10.1038/s41598-018-25862-2.

Newhall, C. G., and S. Self, 1982: The volcanic explosivity index (VEI) an estimate of explosive magnitude for historical volcanism. *J. Geophys. Res. Oceans*, **87**, 1231–1238, https://doi.org/10.1029/JC087iC02p01231.

Ohgaito, R., A. Yamamoto, T. Hajima, R. O'ishi, M. Abe, H. Tatebe, A. Abe-Ouchi, and M. Kawamiya, 2021: PMIP4 experiments using MIROC-ES2L Earth system model. *Geosci. Model Dev.* **14**, 1195–1217, https://doi.org/10.5194/gmd-14-1195-2021.

Olonscheck, D., A. P. Schurer, L. Lücke, and G. C. Hegerl, 2021: Large-scale emergence of regional changes in year-to-year temperature variability by the end of the 21st century. *Nat. Commun.*, **12**, 7237, https://doi.org/10.1038/s41467-021-27515-x.

Oppenheimer, C., 2003: Climatic, environmental and human consequences of the largest known historic eruption: Tambora volcano (Indonesia) 1815. *Prog. Phys. Geog.*, **27**, 230–259, https://doi.org/10.1191/0309133303pp379ra.

Accepted for publication in *Journal of Climate*. DOI 10.1175/JCLI-D-23-0107.1.

Ortega, P., F. Lehner, D. Swingedouw, V. Masson-Delmotte, C. C. Raible, M. Casado, and P. Yiou, 2015: A model-tested North Atlantic Oscillation reconstruction for the past millennium. *Nature*, **523**, 71–74, https://doi.org/10.1038/nature14518.

PAGES 2k Consortium, 2019: Consistent multidecadal variability in global temperature reconstructions and simulations over the Common Era. *Nat. Geosci.*, **12**, 643–649, https://doi.org/10.1038/s41561-019-0400-0.

Paik, S., and S.-K. Min, 2018: Assessing the impact of volcanic eruptions on climate extremes using CMIP5 models. *J. Climate*, **31**, 5333–5349, https://doi.org/10.1175/JCLI-D-17-0651.1.

Pausata, F. S. R., A. Grini, R. Caballero, A. Hannachi, and Ø. Seland, 2015: High-latitude volcanic eruptions in the Norwegian Earth System Model: the effect of different initial conditions and of the ensemble size. *Tellus B*, **67**, 26728, https://doi.org/10.3402/tellusb.v67.26728.

——, C. Karamperidou, R. Caballero, and D. S. Battisti, 2016: ENSO response to high-latitude volcanic eruptions in the Northern Hemisphere: The role of the initial conditions. *Geophys. Res. Lett.*, **43**, 8694–8702, https://doi.org/10.1002/2016GL069575.

Písek, J., and R. Brázdil, 2006: Responses of large volcanic eruptions in the instrumental and documentary climatic data over Central Europe. *Int. J. Climatol.*, **26**, 439–459, https://doi.org/10.1002/joc.1249.

Rao, M. P., E. R. Cook, B. I. Cook, K. J. Anchukaitis, R. D. D'Arrigo, P. J. Krusic, and A. N. LeGrande, 2019: A double bootstrap approach to Superposed Epoch Analysis to evaluate response uncertainty. *Dendrochronologia*, **55**, 119–124, https://doi.org/10.1016/j.dendro.2019.05.001.

Rayner, N. A., D. E. Parker, E. B. Horton, C. K. Folland, L. V. Alexander, D. P. Rowell, E. C. Kent, and A. Kaplan, 2003: Global analyses of sea surface temperature, sea ice, and night marine air temperature since the late nineteenth century. *J. Geophys. Res. Atmos.*, **108**, 4407, https://doi.org/10.1029/2002JD002670.

Robock, A., 2000: Volcanic eruptions and climate. *Rev. Geophys.*, **38**, 191–219, https://doi.org/10.1029/1998RG000054.

Accepted for publication in *Journal of Climate*. DOI 10.1175/JCLI-D-23-0107.1.

——, and J. Mao, 1995: The volcanic signal in surface temperature observations. *J. Climate*, **8**, 1086–1103, https://doi.org/10.1175/1520-0442(1995)008<1086:TVSIST>2.0.CO;2.

Rydval, M., and Coauthors, 2018: Influence of sampling and disturbance history on climatic sensitivity of temperature-limited conifers. *Holocene*, **28**, 1574–1587, https://doi.org/10.1177/0959683618782605.

Schmidt, A., and B. A. Black, 2022: Reckoning with the rocky relationship between eruption size and climate response: toward a volcano-climate index. *Annu. Rev. Earth Planet. Sci.*, **50**, 627–661, https://doi.org/10.1146/annurev-earth-080921-052816.

Schmidt, G. A., and Coauthors, 2011: Climate forcing reconstructions for use in PMIP simulations of the last millennium (v1.0). *Geosci. Model Dev.*, **4**, 33–45, https://doi.org/10.5194/gmd-4-33-2011.

Schneider, L., J. E. Smerdon, U. Büntgen, R. J. S. Wilson, V. S. Myglan, A. V. Kirdyanov, and J. Esper, 2015: Revising midlatitude summer temperatures back to A.D. 600 based on a wood density network. *Geophys. Res. Lett.*, **42**, 4556–4562, https://doi.org/10.1002/2015GL063956.

——, ——, F. Pretis, C. Hartl-Meier, and J. Esper, 2017: A new archive of large volcanic events over the past millennium derived from reconstructed summer temperatures. *Environ. Res. Lett.*, **12**, 094005, https://doi.org/10.1088/1748-9326/aa7a1b.

Schulzweida, U., 2019: CDO User Guide. https://doi.org/10.5281/ZENODO.3539275.

Schurer, A. P., G. C. Hegerl, M. E. Mann, S. F. B. Tett, and S. J. Phipps, 2013: Separating forced from chaotic climate variability over the past millennium. *J. Climate*, **26**, 6954–6973, https://doi.org/10.1175/JCLI-D-12-00826.1.

Sear, C. B., P. M. Kelly, P. D. Jones, and C. M. Goodess, 1987: Global surface-temperature responses to major volcanic eruptions. *Nature*, **330**, 365–367, https://doi.org/10.1038/330365a0.

Sigl, M., and Coauthors, 2015: Timing and climate forcing of volcanic eruptions for the past 2,500 years. *Nature*, **523**, 543–549, https://doi.org/10.1038/nature14565.

Accepted for publication in *Journal of Climate*. DOI 10.1175/JCLI-D-23-0107.1.

Sjolte, J., F. Adolphi, H. Guðlaugsdòttir, and R. Muscheler, 2021: Major differences in regional climate impact between high- and low-latitude volcanic eruptions. *Geophys. Res. Lett.*, **48**, e2020GL092017, https://doi.org/10.1029/2020GL092017.

Smerdon, J. E., 2012: Climate models as a test bed for climate reconstruction methods: pseudoproxy experiments. *Wiley Interdiscip. Rev.: Climate Change*, **3**, 63–77, https://doi.org/10.1002/wcc.149.

Stevenson, S., J. T. Fasullo, B. L. Otto-Bliesner, R. A. Tomas, and C. Gao, 2017: Role of eruption season in reconciling model and proxy responses to tropical volcanism. *Proc. Natl. Acad. Sci. USA*, **114**, 1822–1826, https://doi.org/10.1073/pnas.1612505114.

Swingedouw, D., J. Mignot, P. Ortega, M. Khodri, M. Menegoz, C. Cassou, and V. Hanquiez, 2017: Impact of explosive volcanic eruptions on the main climate variability modes. *Global Planet. Change*, **150**, 24–45, https://doi.org/10.1016/j.gloplacha.2017.01.006.

Tejedor, E., N. Steiger, J. E. Smerdon, R. Serrano-Notivoli, and M. Vuille, 2021: Global temperature responses to large tropical volcanic eruptions in paleo data assimilation products and climate Model simulations over the last millennium. *Paleoceanogr. Paleoclimatol.*, **36**, e2020PA004128, https://doi.org/10.1029/2020PA004128.

Toohey, M., and M. Sigl, 2017: Volcanic stratospheric sulfur injections and aerosol optical depth from 500 BCE to 1900 CE. *Earth Syst. Sci. Data*, **9**, 809–831, https://doi.org/10.5194/essd-9-809-2017.

——, K. Krüger, U. Niemeier, and C. Timmreck, 2011: The influence of eruption season on the global aerosol evolution and radiative impact of tropical volcanic eruptions. *Atmos. Chem. Phys.*, **11**, 12351–12367, https://doi.org/10.5194/acp-11-12351-2011.

——, ——, M. Sigl, F. Stordal, and H. Svensen, 2016: Climatic and societal impacts of a volcanic double event at the dawn of the Middle Ages. *Climatic Change*, **136**, 401–412, https://doi.org/10.1007/s10584-016-1648-7.

——, ——, H. Schmidt, C. Timmreck, M. Sigl, M. Stoffel, and R. Wilson, 2019: Disproportionately strong climate forcing from extratropical explosive volcanic eruptions. *Nat. Geosci.*, **12**, 100–107, https://doi.org/10.1038/s41561-018-0286-2.

Accepted for publication in *Journal of Climate*. DOI 10.1175/JCLI-D-23-0107.1.

Wallace, J. M., and D. S. Gutzler, 1981: Teleconnections in the Geopotential Height Field during the Northern Hemisphere winter. *Mon. Wea. Rev.* **109**, 784–812, https://doi.org/10.1175/1520-0493(1981)109<0784:TITGHF>2.0.CO;2.

Wang, F., D. Arseneault, É. Boucher, G. Galipaud Gloaguen, A. Deharte, S. Yu, and N. Troukechout, 2020: Temperature sensitivity of blue intensity, maximum latewood density, and ring width data of living black spruce trees in the eastern Canadian taiga. *Dendrochronologia*, **64**, 125771, https://doi.org/10.1016/j.dendro.2020.125771.

——, ——, ——, F. Gennaretti, S. Yu, and T. Zhang, 2022: Tropical volcanoes synchronize eastern Canada with Northern Hemisphere millennial temperature variability. *Nat. Commun.*, **13**, 5042, https://doi.org/10.1038/s41467-022-32682-6.

Wilson, R., and Coauthors, 2016: Last millennium northern hemisphere summer temperatures from tree rings: Part I: The long term context. *Quat. Sci. Rev.*, **134**, 1–18, https://doi.org/10.1016/j.quascirev.2015.12.005.

Wunderlich, F., and D. M. Mitchell, 2017: Revisiting the observed surface climate response to large volcanic eruptions. *Atmos. Chem. Phys.*, **17**, 485–499, https://doi.org/10.5194/acp-17-485-2017.

Yukimoto, S., and Coauthors, 2019: The Meteorological Research Institute Earth System Model version 2.0, MRI-ESM2.0: Description and basic evaluation of the physical component. *J. Meteor. Soc. Japan Ser. II*, 931-965, https://doi.org/10.2151/jmsj.2019-051.

Zambri, B., and A. Robock, 2016: Winter warming and summer monsoon reduction after volcanic eruptions in Coupled Model Intercomparison Project 5 (CMIP5) simulations. *Geophys. Res. Lett.*, **43**, 10,920-10,928, https://doi.org/10.1002/2016GL070460.

Zanchettin, D., and Coauthors, 2022: Effects of forcing differences and initial conditions on inter-model agreement in the VolMIP volc-Pinatubo-full experiment. *Geosci. Model Dev.*, **15**, 2265–2292, https://doi.org/10.5194/gmd-15-2265-2022.

Zhong, Y., A. Jahn, G. H. Miller, and A. Geirsdottir, 2018: Asymmetric cooling of the Atlantic and Pacific Arctic during the past two millennia: A dual observation-modeling study. *Geophys. Res. Lett.*, **45**, 12497–12505, https://doi.org/10.1029/2018GL079447.

Accepted for publication in *Journal of Climate*. DOI 10.1175/JCLI-D-23-0107.1.

Zhu, F., J. Emile-Geay, G. J. Hakim, J. King, and K. J. Anchukaitis, 2020: Resolving the differences in the simulated and reconstructed temperature response to volcanism. *Geophys. Res. Lett.*, **47**, e2019GL086908, https://doi.org/10.1029/2019GL086908.

——, ——, K. J. Anchukaitis, G. J. Hakim, A. T. Wittenberg, M. S. Morales, M. Toohey, and J. King, 2022: A re-appraisal of the ENSO response to volcanism with paleoclimate data assimilation. *Nat. Commun.*, **13**, 747, https://doi.org/10.1038/s41467-022-28210-1.

Zhuo, Z., I. Kirchner, S. Pfahl, and U. Cubasch, 2021: Climate impact of volcanic eruptions: the sensitivity to eruption season and latitude in MPI-ESM ensemble experiments. *Atmos. Chem. Phys.*, **21**, 13425–13442, https://doi.org/10.5194/acp-21-13425-2021.

Ziegler, E., and K. Rehfeld, 2021: TransEBM v. 1.0: description, tuning, and validation of a transient model of the Earth's energy balance in two dimensions. *Geosci. Model Dev.*, **14**, 2843–2866, https://doi.org/10.5194/gmd-14-2843-2021.

Accepted for publication in *Journal of Climate*. DOI 10.1175/JCLI-D-23-0107.1.